

①

**AD-A280 476**



**PL-TR-93-2224**

**Environmental Research Papers, No. 1132**

**ATMOSPHERIC STRUCTURE SIMULATION: AN ARMA MODEL  
FOR SMOOTH ISOTROPIC TWO-DIMENSIONAL  
GEOPHYSICAL POWER SPECTRA**

**James H. Brown**

**5 October 1993**

*DTIC QUALITY INSPECTED 2*

**APPROVED FOR PUBLIC RELEASE; DISTRIBUTION UNLIMITED**

**94-18865**



**DTIC  
ELECTE  
JUN 20 1994  
S G D**

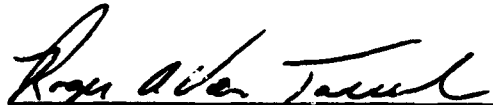


**PHILLIPS LABORATORY  
Directorate of Geophysics  
AIR FORCE MATERIEL COMMAND  
HANSCOM AIR FORCE BASE, MA 01731-3010**

**94 6 17 033**

**"This technical report has been reviewed and is approved for publication"**

  
**William Blumberg**  
**Simulations Branch**  
**Branch Chief**

  
**Roger VanTassel**  
**Optical Environment Division**  
**Division Director**

**This report has been reviewed by the ESC Public Affairs Office (PA) and is releasable to the National Technical Information Service (NTIS)**

**Qualified requestors may obtain additional copies from the Defense Technical Information Center. All others should apply to the National Technical Information Service.**

**If your address has changed, or if you wish to be removed from the mailing list, or if the addressee is no longer employed by your organization, please notify PL/TSI, Hanscom AFB, MA 01731-3010. This will assist us in maintaining a current mailing list.**

**Do not return copies of this report unless contractual obligations or notices on a specific document requires that it be returned.**

# REPORT DOCUMENTATION PAGE

*Form Approved*  
OMB No. 0704-0188

Public reporting burden for this collection of information is estimated to average 1 hour per response, including the time for reviewing instructions, searching existing data sources, gathering and maintaining the data needed, and completing and reviewing the collection of information. Send comments regarding this burden estimate or any other aspect of this collection of information, including suggestions for reducing this burden, to Washington Headquarters Services, Directorate for Information Operations and Reports, 1215 Jefferson Davis Highway, Suite 1204, Arlington, VA 22202-4302, and to the Office of Management and Budget, Paperwork Reduction Project (0704-0188), Washington, DC 20503.

<b>1. AGENCY USE ONLY</b> <i>(Leave blank)</i>	<b>2. REPORT DATE</b> 5 October 1993	<b>3. REPORT TYPE AND DATES COVERED</b> Scientific Interim	
<b>4. TITLE AND SUBTITLE</b> Atmospheric Structure Simulation: An ARMA Model for Smooth Isotropic Two- Dimensional Geophysical Power Spectra		<b>5. FUNDING NUMBERS</b> S3110501 (SHARC)	
<b>6. AUTHOR(S)</b> James H. Brown		<b>8. PERFORMING ORGANIZATION REPORT NUMBER</b>  PL-TR-93-2224 ERP, No. 1132	
<b>7. PERFORMING ORGANIZATION NAME(S) AND ADDRESS(ES)</b>  Phillips Laboratory/GPOS 29 Randolph Road Hanscom AFB, MA 01731-3010			
<b>9. SPONSORING/MONITORING AGENCY NAME(S) AND ADDRESS(ES)</b>		<b>10. SPONSORING/MONITORING AGENCY REPORT NUMBER</b>	
<b>11. SUPPLEMENTARY NOTES</b>			
<b>12a. DISTRIBUTION/AVAILABILITY STATEMENT</b>  Approved for Public Release; Distribution Unlimited		<b>12b. DISTRIBUTION CODE</b>	
<b>13. ABSTRACT</b> <i>(Maximum 200 words)</i>  Geophysical phenomena are often characterized by smooth continuous power spectral densities having a negative power law slope. Frequently, Fourier transform analysis has been employed to generate synthetic scenes from pseudorandom arrays by passing the stochastic data through a Fourier filter having the desired power spectral dependency. This report examines the possibility of producing two-dimensional synthetic structure by invoking autoregressive/moving average analysis, as contrasted with the Fourier method. Computations that apply multidimensional fast Fourier transforms to large data arrays consume enormous resources and time. An alternative method is needed to reduce the computational burden, achieve circular symmetry, account for correlations in all directions, and lend itself to producing non-stationary scenes. Future editions of the Phillips Laboratory Strategic High Altitude Atmospheric Radiance Code (SHARC) will feature an ability to calculate structured radiance. The method explored herein provides a process to construct a non-stationary database for SHARC that accurately simulates symmetric two-dimensional geophysical power spectra and takes into account correlations along the line of sight that existing methods approximate.			
<b>14. SUBJECT TERMS</b> Atmospheric structure Power spectral density analysis Two dimensional power spectra		<b>15. NUMBER OF PAGES</b> 72	
		<b>16. PRICE CODE</b>	
<b>17. SECURITY CLASSIFICATION OF REPORT</b>  Unclassified	<b>18. SECURITY CLASSIFICATION OF THIS PAGE</b>  Unclassified	<b>19. SECURITY CLASSIFICATION OF ABSTRACT</b>  Unclassified	<b>20. LIMITATION OF ABSTRACT</b>  SAR

The study shows that the computational burden may be reduced near ground level where correlation lengths are small but greatly increases at high altitude where correlation lengths are large. The paper describes an intermediate step between a one-dimensional auto-regressive model described earlier and a full three-dimensional hybrid structure model to be described in a subsequent paper.

Accession For	
NTIS CRA&I	<input checked="" type="checkbox"/>
DTIC TAB	<input checked="" type="checkbox"/>
Unannounced	<input type="checkbox"/>
Justification .....	
By .....	
Distribution /	
Availability Codes	
Dist	Avail and/or Special
A-1	

## **Contents**

<b>1. INTRODUCTION</b>	<b>1</b>
<b>2. THEORETICAL DISCUSSION</b>	<b>2</b>
<b>3. FILTER CALCULATIONS</b>	<b>4</b>
<b>4. MODEL DISCUSSION AND RESULTS</b>	<b>5</b>
<b>5. SIMULATION - PROCEDURE</b>	<b>23</b>
<b>6. ARMA SIMULATIONS - RESULTS AND DISCUSSION</b>	<b>31</b>
<b>7. CONVENTIONAL SIMULATION - RESULTS AND DISCUSSION</b>	<b>50</b>
<b>8. COMPUTATIONAL BURDEN</b>	<b>54</b>
<b>9. CONCLUSIONS</b>	<b>55</b>
<b>REFERENCES</b>	<b>57</b>
<b>APPENDIX</b>	<b>59</b>

## Illustrations

1. Log-log plot of two-dimensional power spectral density (PSD) versus spatial frequency plotted along a major (North-South or East-West) axis. 8
2. Same as Figure 1, but the spatial frequency is plotted along a diagonal axis. 9
3. Linear two-dimensional contour plot of power spectral density (PSD) versus spatial frequency. 10
4. Same as Figure 3 but the two-dimensional plot is plotted in logarithmic frequency space. 11
5. Same as Figure 2;  $L_c = 32$  km, except 2-D slope = -3. 12
6. Same as Figure 2;  $L_c = 32$  km, except 2-D slope = -3.67 13
7. Same as Figure 3;  $L_c = 32$  km, except 2-D slope = -3.67 14
8. Same as Figure 4;  $L_c = 32$  km, except 2-D slope = -3.67 15
9. Same as Figure 2, except  $L_c = 84$  km and 2-D slope = -2.67 16
10. Same as Figure 2, except  $L_c = 84$  km and 2-D slope = -3 17
11. Same as Figure 2, except  $L_c = 84$  km and 2-D slope = -3.67 18
12. Same as Figure 3, except  $L_c = 84$  km and 2-D slope = -3.67 19
13. Same as Figure 4, except  $L_c = 84$  km and 2-D slope = -3.67 20
14. Same as Figure 1, except number of frequencies,  $N = 1024$ . 21
15. Same as Figure 14, except the order of AR coefficients =  $13 \times 13$ . Order of MA coefficients =  $25 \times 25$ ,  $N = 1024$ . 22
16. Pictorial representation of two-dimensional sheet of Gaussian random numbers. 24
17. Diagram of symmetrical relationships of four quarter-plane AR filters to each other and to the AR full plane region of support. 26
18. Diagram of starting condition for application of first quarter plane AR filter. Example depicted for  $2 \times 2$  AR quarter plane region of support 27
19. Diagram of intermediate step in processing first of four quarter plane initializations.  $2 \times 2$  AR quarter plane example. 28

20. Diagram of starting condition for application of second quarter plane AR filter. Depicted for same 2 x 2 AR quarter plane region of support	29
21. Diagram of starting condition for application of first full plane AR filter. Example depicted for 3 x 3 AR full plane region of support	32
22. Diagram of intermediate step in processing first of 4 x 1 full plane filters (I = 20 is the number of times entire full plane process is repeated). Depicted for 3 x 3 AR full plane region of support.	33
23. Diagram of intermediate step in processing the full plane moving average (MA) filter. Region of support represents a 7 x 7 order filter.	34
24. Log-log plot of two-dimensional power spectral density (PSD) versus spatial frequency plotted along a diagonal. The 1024 x 1024 simulated data set was derived from an original set of 1300 x 1300 random numbers. The "theoretical" 2-D slope is -2.67 and the correlation length $L_c = 32$ km. The order of the AR coefficients = 3 x 3. Order of the MA coefficients = 7 x 7.	35
25. Log-log plot of one-dimensional power spectral density (PSD) versus spatial frequency plotted along a major axis. The 1024 x 1024 simulated data set was derived from an original set of 1300 x 1300 random numbers. The "theoretical" 1-D slope is -1.67 and the correlation length $L_c = 32$ km. The order of the AR coefficients = 3 x 3. Order of the MA coefficients = 7 x 7	37
26. Log-log plot of one-dimensional power spectral density (PSD) versus spatial frequency plotted along a major axis. The 1024 x 1024 simulated data set was derived from an original set of 1300 x 1300 random numbers. The "theoretical" 1-D slope is -1.67 and the correlation length $L_c = 32$ km. The order of the AR coefficients = 3 x 3. Order of the MA coefficients = 7 x 7.	38
27. Same as Figure 24, except 2-D slope = -3.00.	39
28. Same as Figure 24, except 2-D slope = -3.67.	40
29. Log-log plot of two-dimensional power spectral density (PSD) versus spatial frequency plotted along a diagonal. The 1024 x 1024 simulated data set was derived from an original set of 1300 x 1300 random numbers. The "theoretical" 2-D slope is -2.67 and the correlation length $L_c = 84$ km. The order of the AR coefficients = 3 x 3. Order of the MA coefficients = 7 x 7.	42
30. Same as Figure 29, except 2-D slope = -3	43
31. Same as Figure 29, except 2-D slope = -3.67	44
32. Same as Figure 29, except the order of the AR filter = 13 x 13 and the order of the MA filter = 25 x 25 (no DFT low frequency replacement values).	45
33. Same as Figure 29, except the low frequency power has been subtracted from the 1024 x 1024 simulated data.	46

34. Two-dimensional gray scale pictorial representation of 1024 x 1024 ARMA simulated data with low frequencies subtracted. The data set was constructed for  $L_c = 84$  km, 2-D slope =  $-8/3$ , spacing = 100 m, AR order =  $3 \times 3$ , and MA order =  $7 \times 7$ . 47
35. Same as Figure 29, except only the DFT low frequency replacement power values are shown in the simulation. 48
36. Two-dimensional gray scale pictorial representation of 1024 x 1024 ARMA simulated data (corresponds to Figure 29). The data set was constructed for  $L_c = 84$  km, 2-D slope =  $-8/3$ , spacing = 100 m, AR order =  $3 \times 3$ , and MA order =  $7 \times 7$ . 49
37. Log-log plot of two-dimensional power spectral density (PSD) versus spatial frequency plotted along a diagonal. The 1024 x 1024 simulated data set was derived by performing FFT operations on the same set of random numbers as obtained for Figure 29. The "theoretical" 2-D slope is  $-2.67$  and the correlation length  $L_c = 84$  km. 51
38. Log-log plot of one-dimensional power spectral density (PSD) versus spatial frequency plotted along a major axis (corresponds to Figure 37). The "theoretical" 1-D slope is  $-1.67$  and the correlation length  $L_c = 84$  km. 52
39. Two-dimensional gray scale pictorial representation of 1024 x 1024 FFT simulated data (corresponds to Figure 37). The data set was constructed for  $L_c = 84$  km, 2-D slope =  $-8/3$ , spacing = 100 m 53

## **Acknowledgment**

The author *graciously* acknowledges the contributions of Neil Grossbard for the computer programs, computer runs, graphics, and insights into the mathematical analysis that helped make this report possible.

# Atmospheric Structure Simulation: An ARMA Model for Smooth Isotropic Two-Dimensional Geophysical Power Spectra

## 1. INTRODUCTION

Atmospheric fluctuations in wind speed, temperature, and density are characterized by continuous power spectral density functions. For example, two dimensional wind speed PSD's are found to have log-log slopes of about -2.67. Such spectra often are used in simulating an environment or predicting atmospheric structure. Fast Fourier transform analysis provides a means for filtering white noise with spatial filters to simulate a stationary time or spatial data set. In many applications the Fourier transform technique provides adequate processing speed. Atmospheric structure, which is multidimensional and extends over large volumes, is not readily simulated by conventional techniques. For example, stationary baseline Fourier simulation of a two-dimensional vertical sheet using numerical fast complex Fourier transform (FFT) algorithms requires  $\approx 4MN\text{Log}_2(MN)$  multiplications on the two-dimensional random number set. The resulting Fourier transform values then must be multiplied by the desired power spectrum given the required vertical ( $L_{cv}$ ) and horizontal ( $L_{ch}$ ) correlation values and variances ( $\sigma^2$ ) corresponding to a particular altitude. One must then compute the inverse 2-D transform of this array. The total number of computer multiplications for each altitude is  $O(4MN[\text{Log}_2(MN)+1])$ . Since  $L_{cv}$ ,  $L_{ch}$ , and  $\sigma$  vary with altitude,  $M$  2-D sheets must be calculated; resulting in a combined number of multiplications of  $O(4M^2N[\text{Log}_2(MN)+1])$ . If one wishes to simulate a detailed square vertical plane environment having a side of 100 km with 100 m resolution, then  $M = N = 1024$  and the number of multiplications exceed  $9.0 \times 10^{10}$ . A three dimensional analog of this procedure would require  $O(4M^4(3\text{Log}_2(M)+1))$  computer multiplications or  $O(1.4 \times 10^{14})$ . Even high speed computers available today ( $\approx 100$  Mflop/sec) would take  $\approx 378$  hours or 2.25 weeks to produce a single realization. Thus alternative multidimensional techniques available through modern spectral estimation (and perhaps new developments in chaos or wavelet theory) must be exploited to reduce the computational burden.

The Phillips Laboratory Strategic High Altitude Atmospheric Radiance Code (SHARC)<sup>1</sup> uses first principles to calculate point to space and limb viewing atmospheric background infrared radiance and transmittance. Real atmospheric infrared background perturbations occur from fluctuations in temperature and density of the contributing molecular species. Version 4 of the SHARC code envisions a capability to evaluate radiance structure from estimated variances in the standard temperature and density profiles. This report studies the possibility of producing two-dimensional synthetic structure from autoregressive/moving average (ARMA) analysis as contrasted with the Fourier method. The analysis is performed with a view toward producing circularly symmetric power spectral densities that account for isotropic correlations in the horizontal plane, including the line-of-sight, that existing methods approximate.

During the course of the study, it became apparent that low-order auto-regressive (AR) analysis alone was unable to produce two-dimensional power spectra for the large correlation lengths, evident in the upper atmosphere, that matched desired geophysical specifications. The study, therefore, was extended to include full ARMA analysis. Although low order AR analysis could efficiently be used near ground level where correlation lengths typically are small, the larger high altitude correlation lengths called for complete ARMA analysis, where structure simulations required application of a high order recursion technique. As part of an ongoing study, this report describes an intermediate stage between a one-dimensional auto-regressive model described earlier and a full three-dimensional hybrid structure model to be described in a subsequent report. The hybrid model has its bases in the one-dimensional AR model and is suggested naturally by the present work.

## 2. THEORETICAL DISCUSSION

This report is a two-dimensional extension of a previous report<sup>2</sup> that treated one-dimensional simulation from the autoregressive (AR) modeling perspective. Though the theoretical background for one-dimensional analysis can be extended to two dimensions, the method for estimating the ARMA coefficients is treated somewhat differently in this report.

For the two-dimensional case, we wish to simulate a horizontal sheet of stationary data having a constant correlation length ( $L_c$ ), variance ( $\sigma^2$ ), and spatial spectra characterized by the symmetric two-dimensional power spectral density function (PSD):

$$F(f_k) = \frac{\sigma^2 v a^{2v}}{\pi (a^2 + f_k^2)^{v+1}}$$

---

<sup>1</sup>Sharma, R.D., Duff, J.W., Sundberg, R.L., Gruninger, J.H., Bernstein, L.S., Robertson, D.C., and Healey, R.J., (1991) *Description of SHARC-2, The Strategic High Altitude Atmospheric Radiance Code*, Phillips Laboratory technical report, PL-TR-91-2071. ADA239008

<sup>2</sup>Brown, J.H., (1993) *Atmospheric Structure Simulation: An Autoregressive Model for Smooth Geophysical Power Spectra with Known Autocorrelation Function*, Phillips Laboratory technical report, PL-TR-93-2185, ERP #1128. ADA276691

where,

$$a^{-1} = \frac{2\sqrt{\pi}\Gamma(\nu)}{\Gamma\left(\nu + \frac{1}{2}\right)} L_c \quad \text{and where, } f_k^2 = f_x^2 + f_y^2$$

Here,  $f_k$  is the spatial frequency ( $\text{km}^{-1}$ ) and  $-2(\nu+1)$  is the spectral slope of  $\log(F)$  vs  $\log(f_k)$ .

The two-dimensional ARMA power spectral density model is<sup>3,4</sup>:

$$P_{\text{ARMA}}(f_x, f_y) = T_1 T_2 \rho_w \left| \frac{B(f_x, f_y)}{A(f_x, f_y)} \right|^2$$

where the autoregressive factor is,

$$A(f_x, f_y) = \sum_m \sum_n a(m, n) e^{-2\pi i m f_x T_1} e^{-2\pi i n f_y T_2}$$

and the moving average factor is,

$$B(f_x, f_y) = \sum_m \sum_n b(m, n) e^{-2\pi i m f_x T_1} e^{-2\pi i n f_y T_2}$$

$T_1$  and  $T_2$  are the sampling intervals,  $\rho_w$  is the variance of the white noise process, and  $a(m, n)$ ,  $b(m, n)$  are respectively the autoregressive and moving average filter coefficients.

The discrete two-dimensional series,  $x(k, l)$ , that approximates these deterministic and stochastic processes can be simulated by the finite filter difference equation:

$$x(k, l) = - \sum_{\substack{m \\ (m, n) \neq (0, 0)}} \sum_n a(m, n) x[k - m, l - n] + \sum_m \sum_n b(m, n) \epsilon[k - m, l - n]$$

in which the range of summations denote the order of the 2D difference equation. In this report, the order of the arrays  $a(m, n)$  and  $b(m, n)$  are  $(2M+1) \times (2N+1)$  where the region of support is the square full plane covering  $-M \leq m \leq M$  and  $-N \leq n \leq N$  and where  $M = N$ . The output sequence is  $x(k, l)$ , and  $\epsilon(k, l)$  is a white noise input driving sequence. The  $a(m, n)$  autoregressive coefficients were calculated from an auto-regressive estimator and the  $b(m, n)$  moving average coefficients were calculated from the equivalent MA filter.<sup>5</sup>

<sup>3</sup>Marple, S.L. (1987) *Digital Spectral Analysis with Applications*, Chapter 6, Prentice-Hall, Englewood Cliffs, New Jersey.

<sup>4</sup>Key, Steven M. (1988) *Modern Spectral Estimation, Theory & Application*, Prentice-Hall, Englewood Cliffs, New Jersey.

<sup>5</sup>Lim, J.S. (1990) *Two-Dimensional Signal and Image Processing*, Prentice-Hall, Englewood Cliffs New Jersey, pg 269.

### 3. FILTER CALCULATIONS

Let us first treat the autoregressive factor in a region of full plane support.

$$A(f_x, f_y) = \sum_{m=-M}^M \sum_{n=-N}^N a(m, n) e^{-2\pi i [m f_x T_1 + n f_y T_2]}$$

Considering the 8-fold symmetries of the present problem, the following relationships apply:

$$\begin{aligned} a(m, n) &= a(-m, n) = a(m, -n) = a(-m, -n) \\ &= a(n, m) = a(-n, m) = a(n, -m) = a(-n, -m), \end{aligned}$$

with similar symmetries for the b's. And we define  $a(0,0) = 1$ .

Due to these symmetries,  $A(f_x, f_y)$ , and in a similar way  $B(f_x, f_y)$ , can be written as:

$$A(f_x, f_y) = \sum_{m=1}^M \sum_{n=-N}^N a(m, n) \left\{ e^{-2\pi i [f_x m T_1 + f_y n T_2]} + e^{-2\pi i [-f_x m T_1 + f_y n T_2]} \right\} + \sum_{n=-N}^N a(0, n) e^{-2\pi i n f_y T_2}$$

Using the identity:  $\cos(x) = \frac{e^{ix} + e^{-ix}}{2}$ , then,

$$A(f_x, f_y) = 2 \sum_{m=1}^M \sum_{n=-N}^N a(m, n) \cos(2\pi f_x m T_1) e^{-2\pi i n f_y T_2} + \sum_{n=-N}^N a(0, n) e^{-2\pi i n f_y T_2}$$

and then similarly,

$$\begin{aligned} A(f_x, f_y) &= 4 \sum_{m=1}^M \sum_{n=1}^N a(m, n) \cos(2\pi f_x m T_1) \cos(2\pi f_y n T_2) \\ &\quad + 2 \sum_{n=1}^N a(0, n) \cos(2\pi f_y n T_2) + 2 \sum_{m=1}^M a(m, 0) \cos(2\pi f_x m T_1) + a(0, 0) \end{aligned}$$

Assume that  $A(f_x, f_y)$  defines a stable filter, then  $A(f_x, f_y) > 0$  for all  $(f_x, f_y)$ ; or,

$$\sqrt{\text{PSD}(f_x, f_y)} = \sqrt{\rho T_1 T_2} \frac{B(f_x, f_y)}{A(f_x, f_y)}$$

We then find an approximate solution for  $A(f_x, f_y)$  by setting  $B(f_x, f_y) = \frac{1}{\sqrt{\rho T_1 T_2}}$ . Then with  $a(0,0) = 1$ , we find  $a(m, n)$  for  $m \geq 0$  and  $n \geq 0$  by solving the following least square problem for a large set of  $f_x, f_y$  values:  $1 = A(f_x, f_y) \sqrt{F(f_k)}$ . The set of "theoretical" PSD's used in solving the least square problem are chosen from 50 circles defined by  $f_k = \sqrt{f_x^2 + f_y^2} = \text{constant}$ , which is equally spaced in  $\text{Log} \sqrt{f_x^2 + f_y^2}$  and by 20 points on each circle defined by 20 equally spaced angles  $\tan^{-1}\left(\frac{f_y}{f_x}\right)$  between 0 and  $\pi/4$ . The minimum frequency,  $(f_k)_{\min}$ , used in the fit is

$(f_k)_{\min} = \frac{1}{N \cdot \text{spacing}}$ , where  $N$  is usually set to 128. In finding  $a(m,n)$  from the least squares procedure, the analysis places a weight of 100x for the minimum frequency.

Having found a least squares solution for  $a(m,n)$ , we proceed as before to solve for

$$B(f_x, f_y) = 4 \sum_{m=1}^M \sum_{n=1}^N b(m,n) \cos(2\pi f_x m T_1) \cos(2\pi f_y n T_1) \\ + 2 \sum_{n=1}^N b(0,n) \cos(2\pi f_y n T_1) + 2 \sum_{m=1}^M b(m,0) \cos(2\pi f_x m T_1) + b(0,0)$$

by setting up the least squares problem:  $1 = \frac{B(f_x, f_y) \sqrt{\rho T_1 T_2}}{A(f_x, f_y) \sqrt{F(f_k)}}$ , where  $A(f_x, f_y)$  are the values found from using the solved set of  $a(m,n)$  values, and where the solution is over a large set of  $f_x, f_y$  values.

#### 4. MODEL DISCUSSION AND RESULTS

The following discussion is aimed at producing a practical two dimensional isotropic autoregressive/moving average (ARMA) model of horizontal atmospheric structure consistent with having a pre-assigned power spectral density. Correlation lengths and  $\sigma^2$  variances are taken from Strugala, et al.<sup>6</sup> In the following discussion the full plane autoregressive  $a(m,n)$  coefficients will be referred to as the AR coefficients and the moving average  $b(m,n)$  coefficients will be referred to as the MA coefficients. The order of the full plane AR or MA calculations will be referred to as having a  $(2M+1) \times (2M+1)$  region of support. Because the region of support has an 8-fold symmetry and the desired 2-D PSD is circularly symmetric, the total number of full plane unique AR or MA coefficients is equal to  $\frac{(M+2)(M+1)}{2}$ ; whereas the total number (non-unique) AR coefficients is equal to  $4M(M+1)$  and the total number of (non-unique) MA coefficients is equal to  $(2M+1)^2$ .

Three model curves are plotted in each of Figures 1-2, 5-6, 9-11, and 14. In these figures, curves marked by an asterisk (\*) at the first frequency are the desired or "theoretical" PSD's (that is,  $F(f_k)$ ). Curves marked by open squares ( $\square$ ) represent the PSD of the full plane autoregressive [AR] predictor model alone  $\left( \text{that is, } \left| \frac{1}{A(f_x, f_y)} \right|^2 \right)$  multiplied by the factor indicated on the plot. Curves marked by an open triangle ( $\Delta$ ) at the first frequency represent the PSD's of the

<sup>6</sup>Strugala, L.A., Newt, J.E., Futterman, W., Schweitzer, E.L., Herman, B.J., and Sears, R.D.(1991) Development of High Resolution Statistically Non-stationary Infrared Earthlimb Radiance Scenes, *Characterization, Propagation, and Simulation of Sources and Backgrounds, Proceedings SPIE - The International Society for Optical Engineering*, V1486, pp 176-187, April 1991, Orlando, Florida.

full ARMA predictor model  $\left( \text{that is, } \left( \rho T_1 T_2 \left| \frac{B(f_x, f_y)}{A(f_x, f_y)} \right|^2 \right) \right)$ , which is to say, the AR model corrected by

the moving average [MA] model). Except where otherwise noted, the sampling spacing is 100 m,  $N$  for determination of the minimum frequency = 128, and the Nyquist frequency is  $5 \text{ km}^{-1}$ . This means that the "minimum" frequency that went into calculating the AR and MA coefficients was  $f_{\text{min}} = \frac{1}{N\Delta x} \approx 0.078 \text{ km}^{-1}$ . In the model plots, this point is marked by the left-most X. Figure 1 is typical of the model plots in this report showing log-log power spectral densities (PSD's). This and subsequent two-dimensional power spectral density plots have PSD's measured in  $\frac{(\delta T / \text{Temperature})^2}{\text{Wavenumber}^2}$  and wavenumber measured in  $\text{km}^{-1}$ . The input parameters for Figure 1 are  $L_{\text{ch}} = 32 \text{ km}$ ,  $\sigma^2 = 0.02$ , and spectral slope (S) =  $-8/3$ . This plot was calculated along a principal axis using a  $3 \times 3$  order AR calculation and a  $7 \times 7$  order MA calculation. Except for a small amount of overshoot at low frequencies ( $\approx 0.2\text{-}0.3 \text{ km}^{-1}$ ), agreement between desired and predicted PSD is good. Since the ARMA PSD model can be calculated at any frequency, this and subsequent figures show the expected bias between the desired and predicted PSD below the "minimum" frequency. Figure 2, which is evaluated along a diagonal axis, shows similar results and verifies the circular symmetry of the 2D ARMA PSD. Further evidence of the near circular symmetry is shown in Figure 3, which displays contours of constant PSD in two-dimensional linear frequency space. Although perfectly symmetrical, the contours exhibit deviations from perfect circularity. For the most part, these deviations are suppressed when plotted in log-log frequency space as shown in Figure 4.

Figures 5 and 6 use the same parameters as Figure 2, except that Figure 5 is evaluated for a slope of  $-3$  and Figure 6 is evaluated for a slope of  $-11/3$ . These plots indicate that slightly better agreement obtains between the "theoretical" and model curves as the spectral slope steepens. Also the "DC" bias diminishes with steeper slope. Figures 7 and 8 show constant contours of the  $-11/3$  model PSD plotted in two-dimensional linear space and two-dimensional log-log space respectively. Comparing these to Figures 3 and 4, we see that slightly better circularity evidently obtains at the steeper slope.

Figures 9, 10, and 11 repeat the input parameters of Figures 2, 5, and 6, except that  $L_{\text{ch}}$  is increased to 84 km and  $\sigma^2$  is decreased to 0.005. Again slightly better agreement obtains as the slope steepens from  $-8/3$  in Figure 9 to  $-3$  in Figure 10 to  $-11/3$  in Figure 11. In fact, agreement is particularly good at the "minimum" frequency for the  $-11/3$  slope. Figures 12 and 13 which show, respectively, two-dimensional linear and log-log frequency plots of constant PSD contours for  $L_{\text{ch}} = 84 \text{ km}$  and  $-11/3$  spectral slope, are comparable to the  $L_{\text{ch}} = 32 \text{ km}$  contour plots of Figures 7 and 8.

Figure 14 repeats the calculation of Figure 1 for  $L_{\text{ch}} = 32 \text{ km}$ , 2-D slope =  $-8/3$ , but now  $N = 1024$ . Clearly the low order ARMA model does not provide good agreement for the wider frequency range. Figure 15 provides an indication of the results of using higher order AR and MA models. The curves in Figure 15 also are calculated for  $L_{\text{ch}} = 32 \text{ km}$ , 2-D slope =  $-8/3$ , and  $N = 1024$ , and thus may be compared with Figure 14. Comparing just the AR curves, we observe that as the

order of the AR process increases from 3 x 3 (Figure 14) to 13 x 13 (Figure 15): the low frequency "rollover" occurs at smaller frequencies, and the number of "ripples" increase. Comparing the complete ARMA curves, we observe that as the order of the AR process increases from 3 x 3 to 13 x 13 and as the order of the MA process increases from 7 x 7 to 25 x 25: the "theoretical" and model PSD's agree much better at low frequency, the "DC" bias decreases, and the amplitude of the "ripples" decrease. As observed, PSD's having a small slope, large correlation length, and small data spacing are more difficult to model than PSD's with larger slope, smaller correlation length, and wider data spacing.

The analysis indicates that two-dimensional isotropic horizontal atmospheric temperature structure, having a data spacing of 100 m and a characteristically smooth power spectral density can be modeled within a frequency band ranging from  $0.08 \text{ km}^{-1}$  to  $5 \text{ km}^{-1}$  by an autoregressive 3 x 3 order process and a moving average 7 x 7 order process. At the expense of increasing computer time, one may increase the frequency range and achieve agreement to  $0.01 \text{ km}^{-1}$  by choosing a 13 x 13 AR model and 25 x 25 MA model.

LC= 9.80E-01 SIGMA= 2.00E-01 SLOPE OF PSD=-2.67  
 A= 3.71E-09 WEIGHT LEAST PSD BY: 0.0E+00  
 AR ORDER 3 x 3 MA ORDER 7 x 7  
 MIN. FRE. of FIT= 7.01E-02 WAVE NUMBER AND ON: 1.00E-01

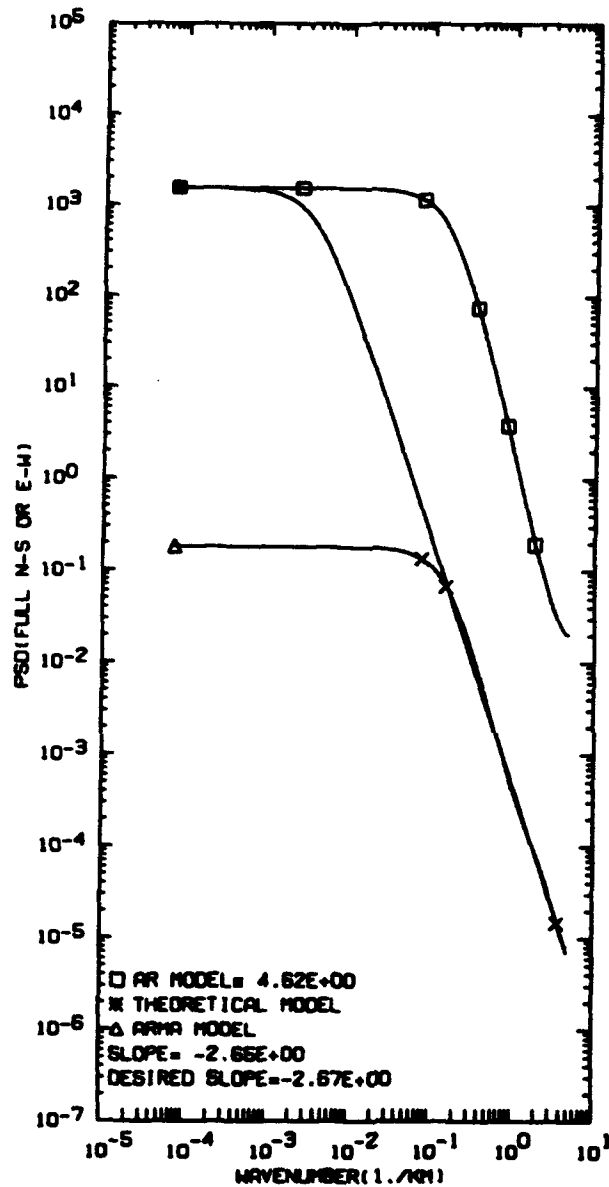


Figure 1. Log-log plot of two-dimensional power spectral density (PSD) versus spatial frequency plotted along a major (North-South or East-West) axis. Curve marked by an asterisk (\*) at the first frequency is the desired or "theoretical" PSD. Curve marked by open squares (o) represents the PSD of the full plane auto-regressive [AR] predictor model multiplied by the factor indicated on the plot. Curve marked by an open triangle ( $\Delta$ ) at the first frequency represents the PSD of the full ARMA predictor model (which is to say, the AR model corrected by the moving average [MA] model; this model is found by weighted least squares fit where the minimum frequency of the fit is  $\frac{1}{N \cdot \text{spacing}}$ ). The 2-D slope is -2.67 and the correlation length  $L_c = 32$  km. The spacing in this and all subsequent PSD's = 100 m. Order of AR coefficients = 3 x 3. Order of MA coefficients = 7 x 7.  $N = 128$  in this and other plots unless otherwise noted

LC= 3.80E-01 SIGMA= 2.00E-01 SLOPE OF PSD=2.67  
 AN= 3.71E-03 MEAN LAGST PRED BY 1.00E-02  
 AR ORDER 3 X 3 MA ORDER 7 X 7  
 RMS PRE. AL/INSTR= 7.84E-02 MORE INFO AND ETC. 1.00E-01

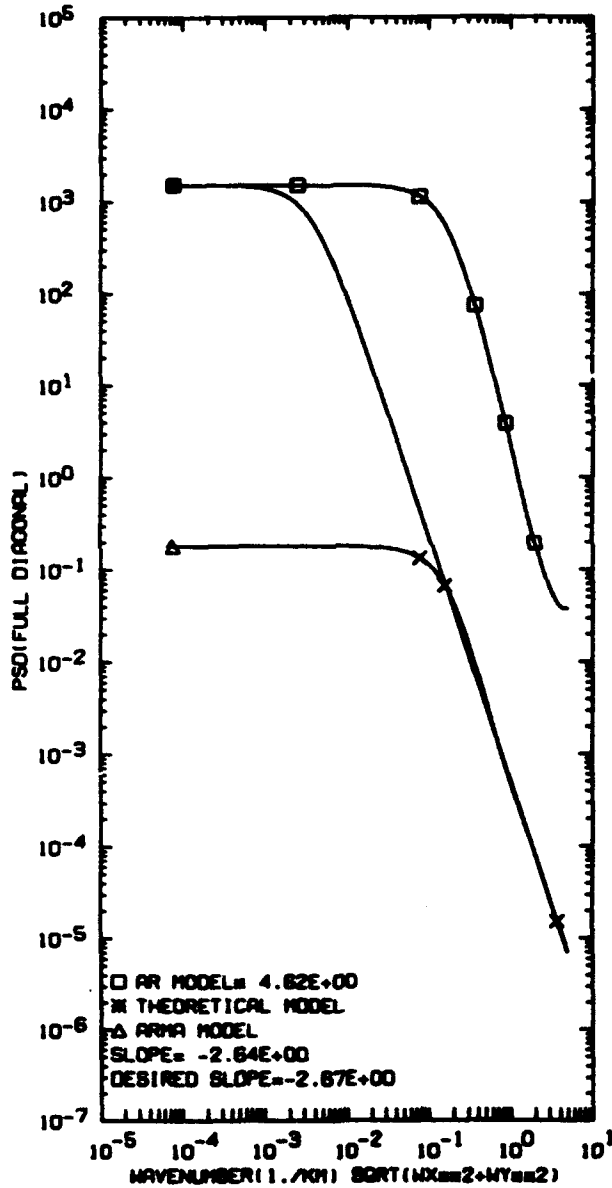
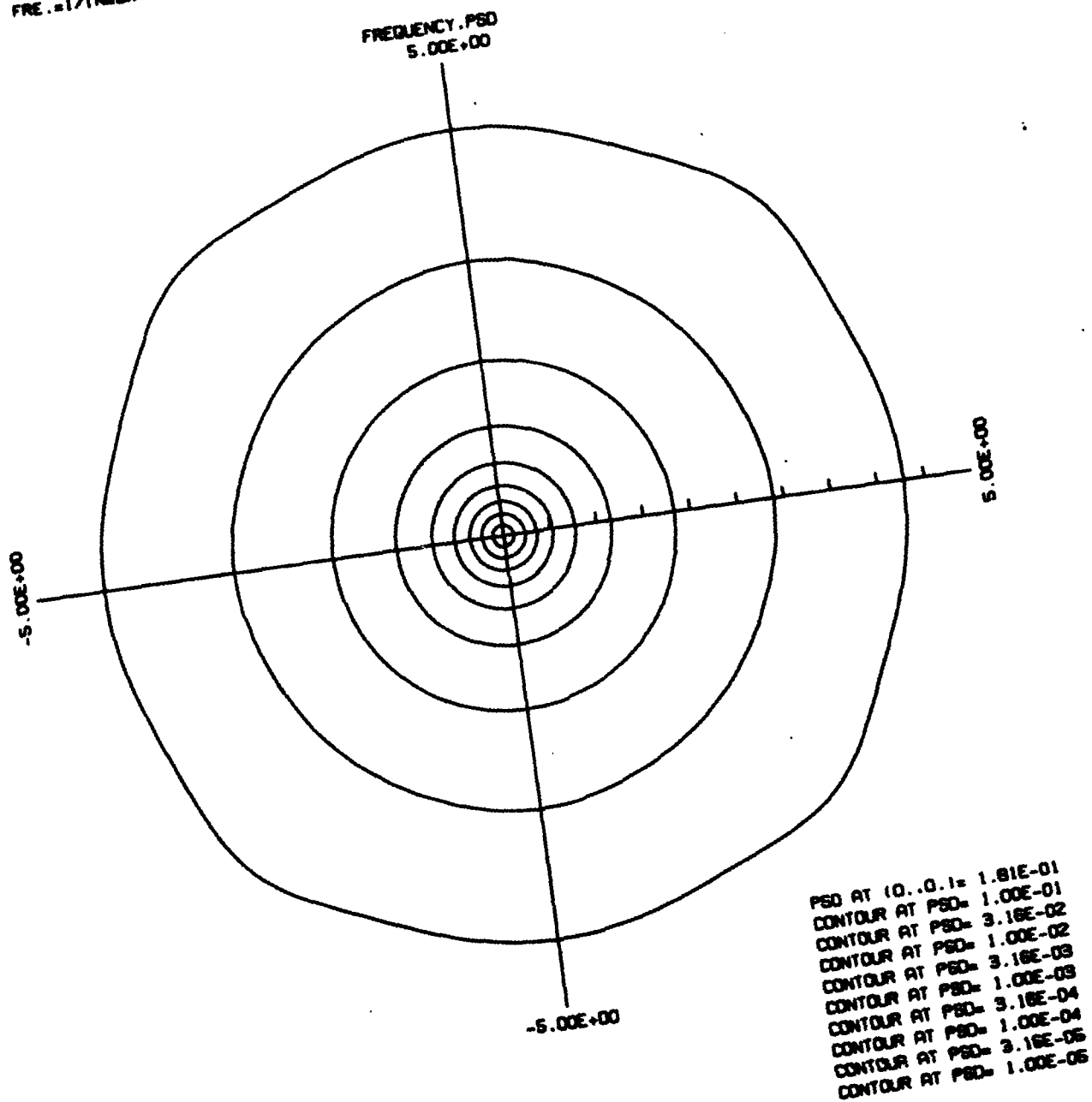


Figure 2. Same as Figure 1, but the spatial frequency is plotted along a diagonal axis

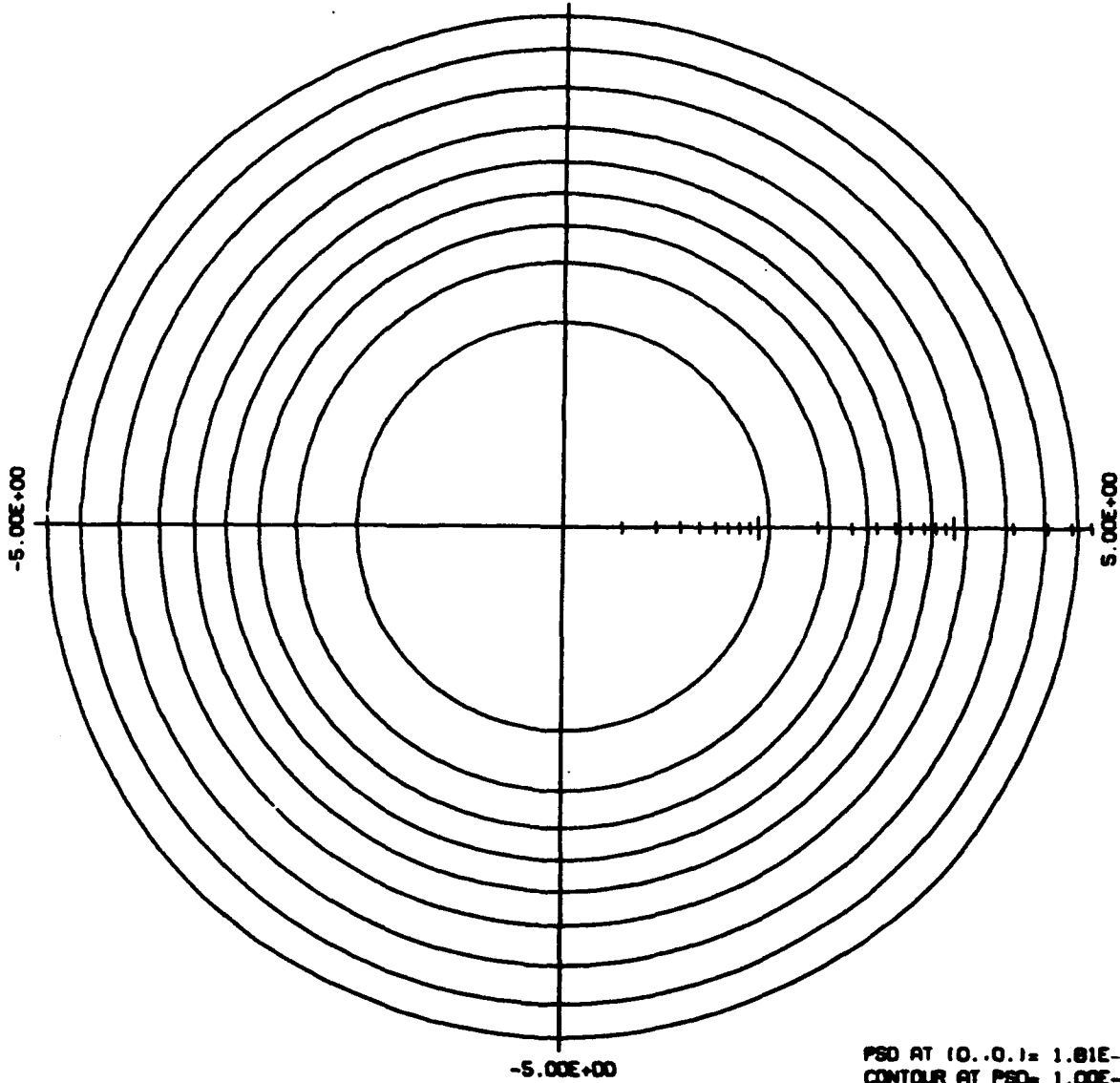
$L_C = 3.20E+01$   $SLOPE_{2D} = 2.00E-01$   $SLOPE\ OF\ PSD = 2.67$   
 $R = 3.71E-03$   $WEIGHT\ LOWEST\ FREQ\ BY\ 1.00E+02$   
 $AR\ ORDER\ 3\ X\ 3$   $MA\ ORDER\ 7\ X\ 7$   
 $MIN.\ FREQ. = 1/(N\Delta X)$   $WHERE\ N = 128$   $AND\ \Delta X = 1.00E-01$   $MIN.\ FREQ. = 7.81E-02$



**Figure 3. Linear two-dimensional contour plot of power spectral density (PSD) versus spatial frequency. Curves represent constant PSD contours of the full ARMA predictor model. The 2-D slope is -2.67 and the correlation length  $L_C = 32$  km. Order of AR coefficients =  $3 \times 3$ . Order of MA coefficients =  $7 \times 7$**

LC= 3.20E+01 SIGMA=2= 2.00E-01 SLOPE OF PSD=2.67  
 A= 3.71E-03 WEIGHT LOWEST FREQ BY 1.00E+02  
 AR ORDER 3 X 3 MA ORDER 7 X 7  
 MIN. FRE.=1/(N\*DX) WHERE N=128 AND DX= 1.00E-01 MIN. FRE.= 7.81E-02

LOG(FREQUENCY).PSD WITH CENTER FREQUENCY= 1.00E-02  
 5.00E+00



PSD AT 10.01= 1.81E-01  
 CONTOUR AT PSD= 1.00E-01  
 CONTOUR AT PSD= 3.16E-02  
 CONTOUR AT PSD= 1.00E-02  
 CONTOUR AT PSD= 3.16E-03  
 CONTOUR AT PSD= 1.00E-03  
 CONTOUR AT PSD= 3.16E-04  
 CONTOUR AT PSD= 1.00E-04  
 CONTOUR AT PSD= 3.16E-05  
 CONTOUR AT PSD= 1.00E-05

Figure 4. Same as Figure 3 but the two-dimensional plot is plotted in logarithmic frequency space



LC= 3.30E+01 SLOPE= 2.00E-01 SLOPE OF PSD=-3.67  
 R= 8.97E-03 WEIGHT LEAST PRED BY 1.00E+02  
 AR ORDER 3 X 3 AR ORDER 7 X 7  
 MIN PRE.=1/100000 7.81E-02 MORE P=100 AND ON= 1.00E-01

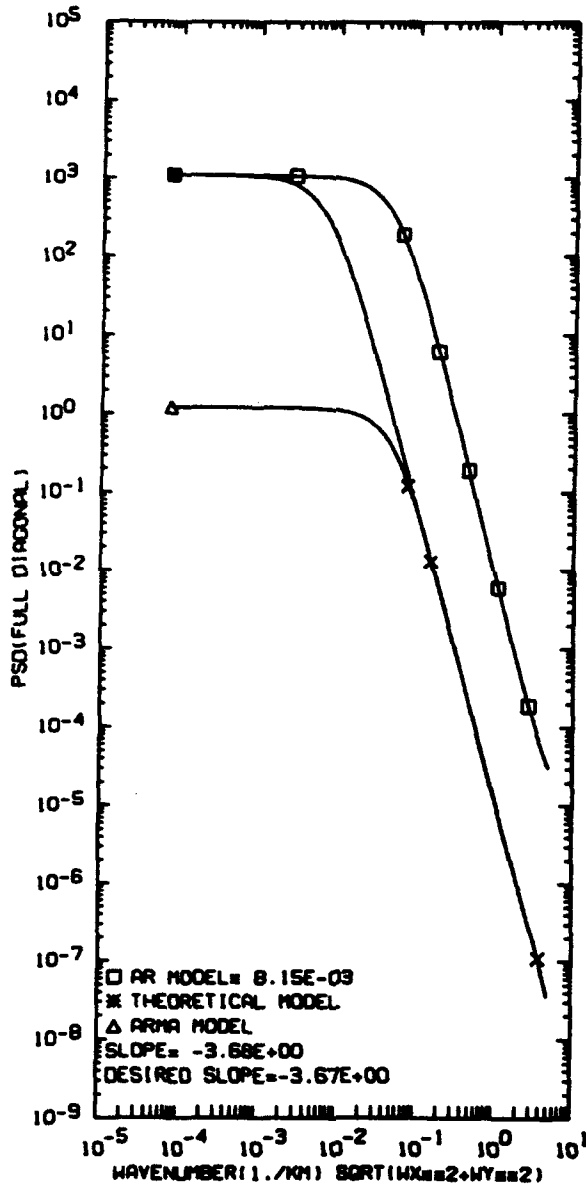


Figure 6. Same as Figure 2;  $L_c = 32$  km, except 2-D slope = -3.67

$L_C = 3.20E+01$   $SIGMA_{rms} = 2 = 2.00E-01$  SLOPE OF PSD = -3.67  
 $A = 6.97E-03$  WEIGHT LOWEST FREQ BY  $1.00E+02$   
 AR ORDER 3 X 3 MA ORDER 7 X 7  
 MIN. FRE. =  $1/(N \cdot \Delta X)$  WHERE  $N = 128$  AND  $\Delta X = 1.00E-01$  MIN. FRE. =  $7.81E-02$

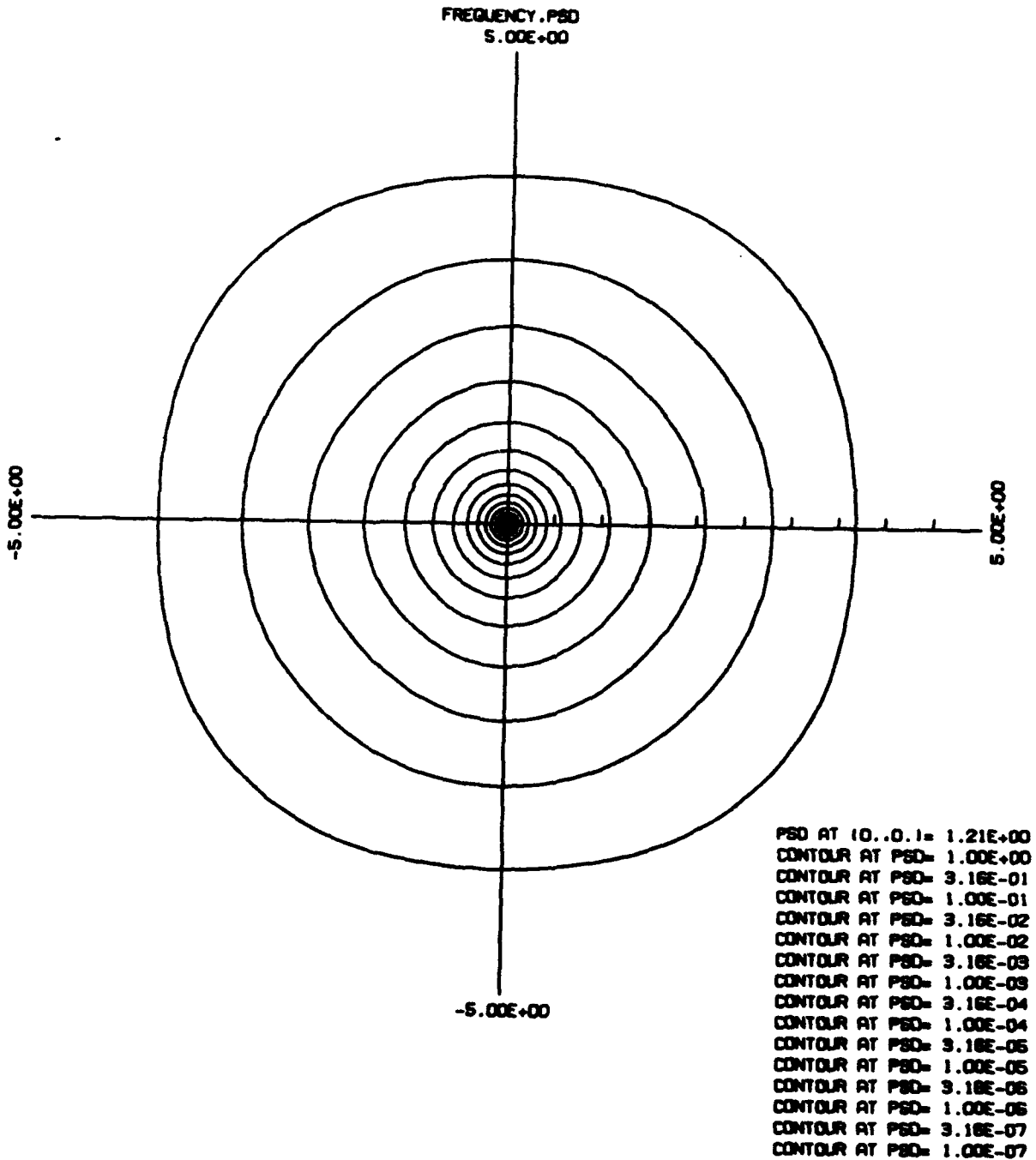


Figure 7. Same as Figure 3;  $L_C = 32$  km, except 2-D slope = -3.67

LC= 3.20E+01 SIGMA=2= 2.00E-01 SLOPE OF PSD=3.67  
 A= 6.97E-03 WEIGHT LOWEST FREQ BY 1.00E+02  
 AR ORDER 3 X 3 MA ORDER 7 X 7  
 MIN. FRE.=1/(N\*DX) WHERE N=128 AND DX= 1.00E-01 MIN. FRE.= 7.81E-02

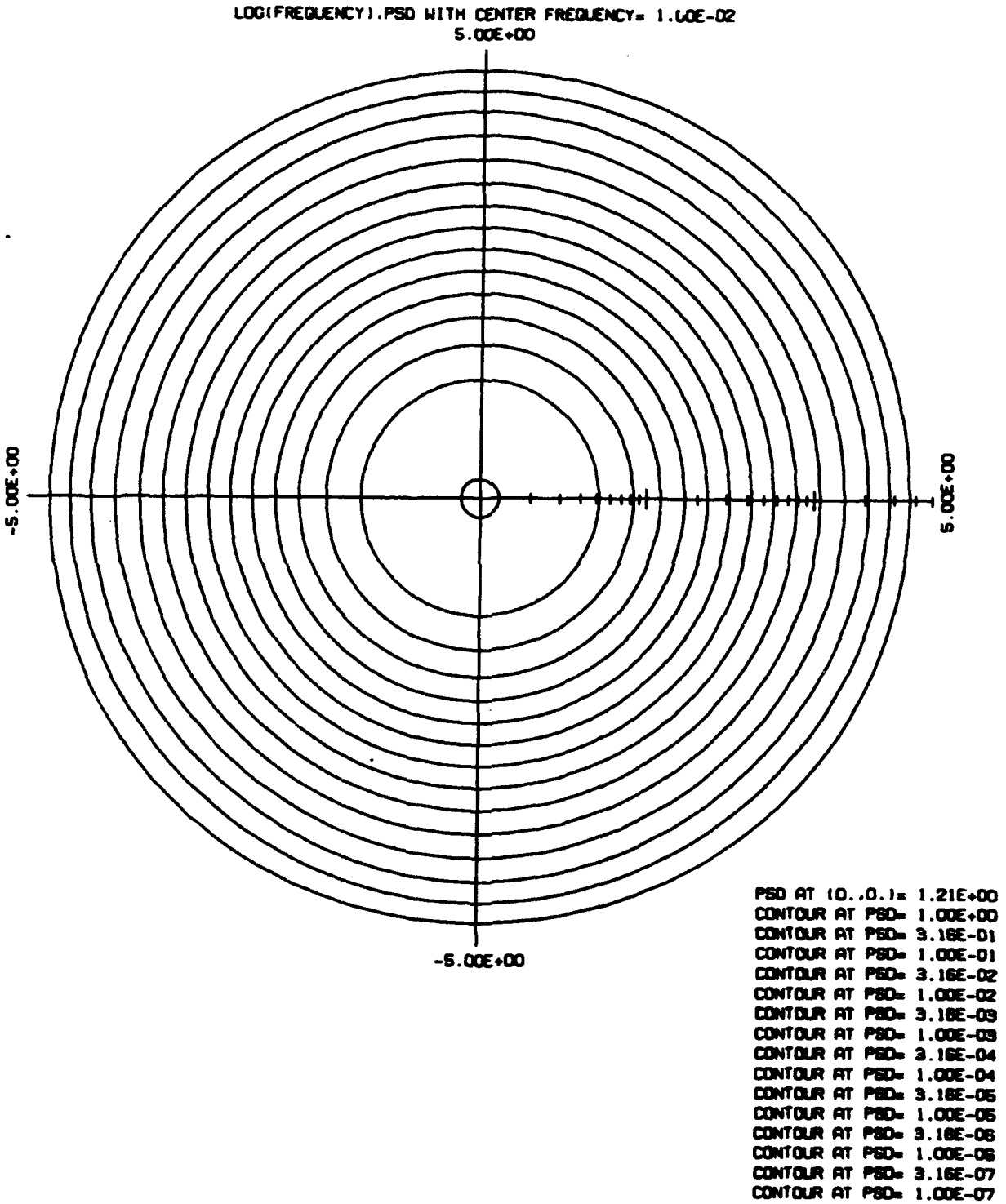


Figure 8. Same as Figure 4;  $L_c = 32$  km, except 2-D slope = -3.67

$L_c = 8.40E+01$   $SIGMA_{w2} = 5.00E-03$  SLOPE OF PSD = -2.67  
 $R = 1.42E-03$  HEIGHT LOWEST PRED BY  $1.00E+02$   
 AR ORDER 3 X 3 MA ORDER 7 X 7  
 NIN PRE. #1/INCH = 7.81E-02 MORE #128 AND ON = 1.00E-01

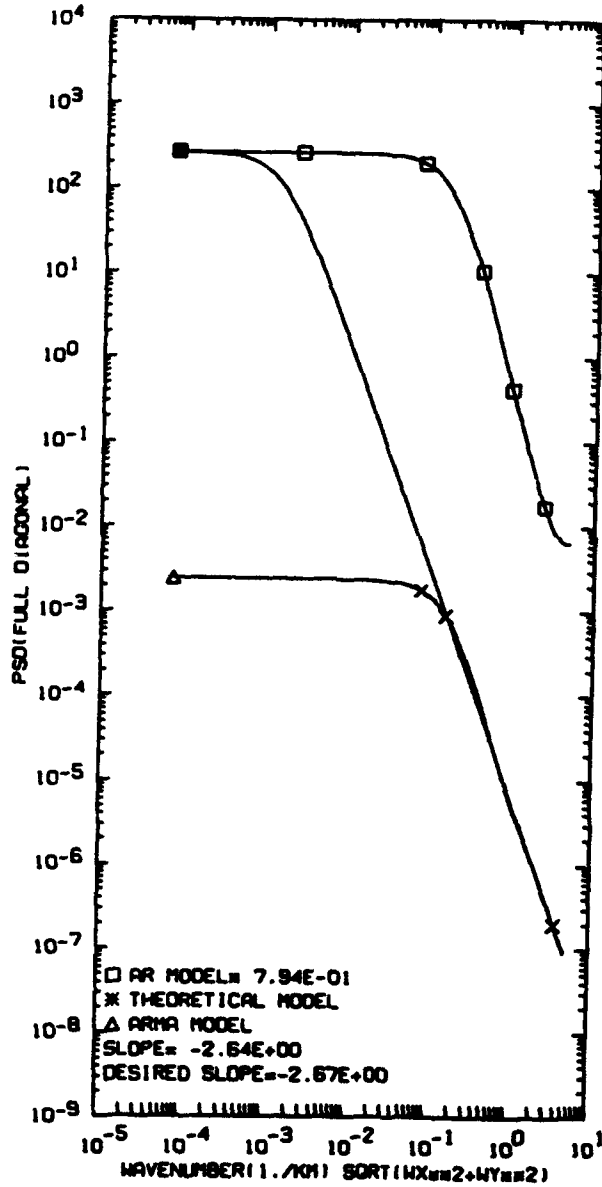


Figure 9. Same as Figure 2, except  $L_c = 84$  km and 2-D slope = -2.67

LC= 8.40E+01 SIGMA= 5.00E-03 SLOPE OF PSD=-3.00  
 R= 1.96E-03 WEIGHT LOWEST FREQ BY 1.00E+02  
 AR ORDER 3 X 3    MA ORDER 7 X 7  
 RIN FREQ. 0.1/1000000 7.81E-02 WHERE N=128    AND ON= 1.00E+01

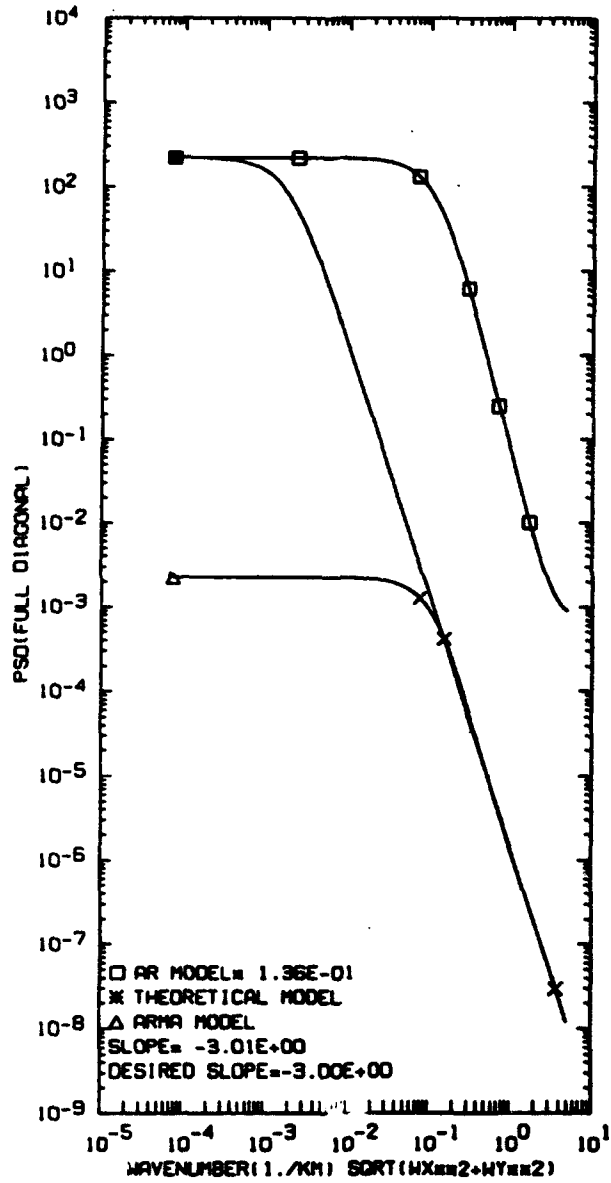


Figure 10. Same as Figure 2, except  $L_c = 84$  km and 2-D slope = -3

$L_c = 8.40E+01$   $SLOPE_{2D} = 5.00E-03$   $SLOPE\ OF\ PSD = -3.67$   
 $R_n = 2.68E-03$   $HEIGHT\ LOWEST\ PRED\ BY = 1.00E-02$   
 $AR\ ORDER\ 3\ X\ 3$   $MA\ ORDER\ 7\ X\ 7$   
 $RIN\ FREQ.\ (1/KH) = 7.81E-02$   $WHERE\ No\ 128$   $AND\ ON = 1.00E-01$

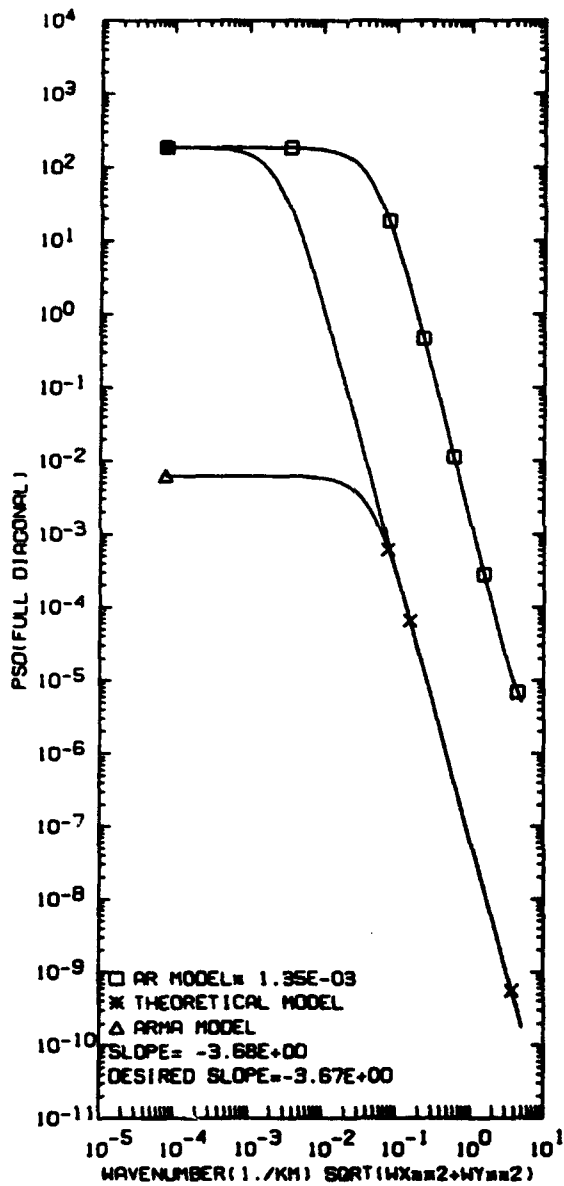


Figure 11. Same as Figure 2, except  $L_c = 84$  km and 2-D slope = -3.67

$L_C = 8.40E+01$   $\text{SIGMA}_{\text{rms}} = 5.00E-09$  SLOPE OF PSD = 3.67  
 $A = 2.66E-03$  WEIGHT LOWEST FREQ BY  $1.00E+02$   
 AR ORDER 3 X 3 MA ORDER 7 X 7  
 MIN. FRE. =  $1/(N \cdot \text{DX})$  WHERE  $N = 128$  AND  $\text{DX} = 1.00E-01$  MIN. FRE. =  $7.81E-02$

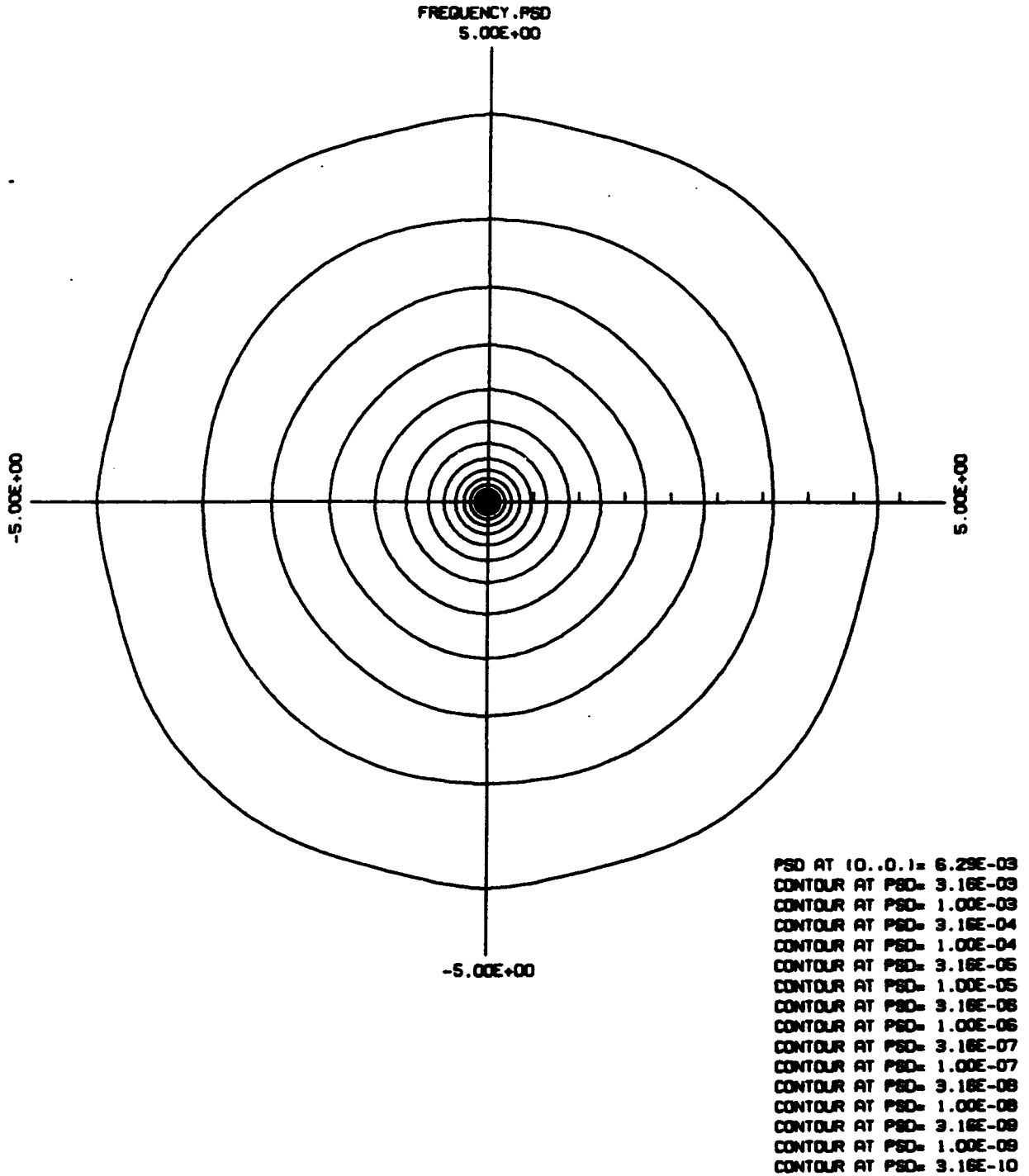


Figure 12. Same as Figure 3, except  $L_C = 84$  km and 2-D slope = -3.67

$L_C = 8.40E+01$   $SIGMA = 2 = 5.00E-03$  SLOPE OF PSD = -3.67  
 $A = 2.66E-03$  WEIGHT LOWEST FREQ BY  $1.00E+02$   
 AR ORDER 3 X 3 NA ORDER 7 X 7  
 MIN. FRE. =  $1/(N \cdot DX)$  WHERE  $N = 128$  AND  $DX = 1.00E-01$  MIN. FRE. =  $7.81E-02$

LOG(FREQUENCY).PSD WITH CENTER FREQUENCY =  $1.00E-02$   
 $5.00E+00$

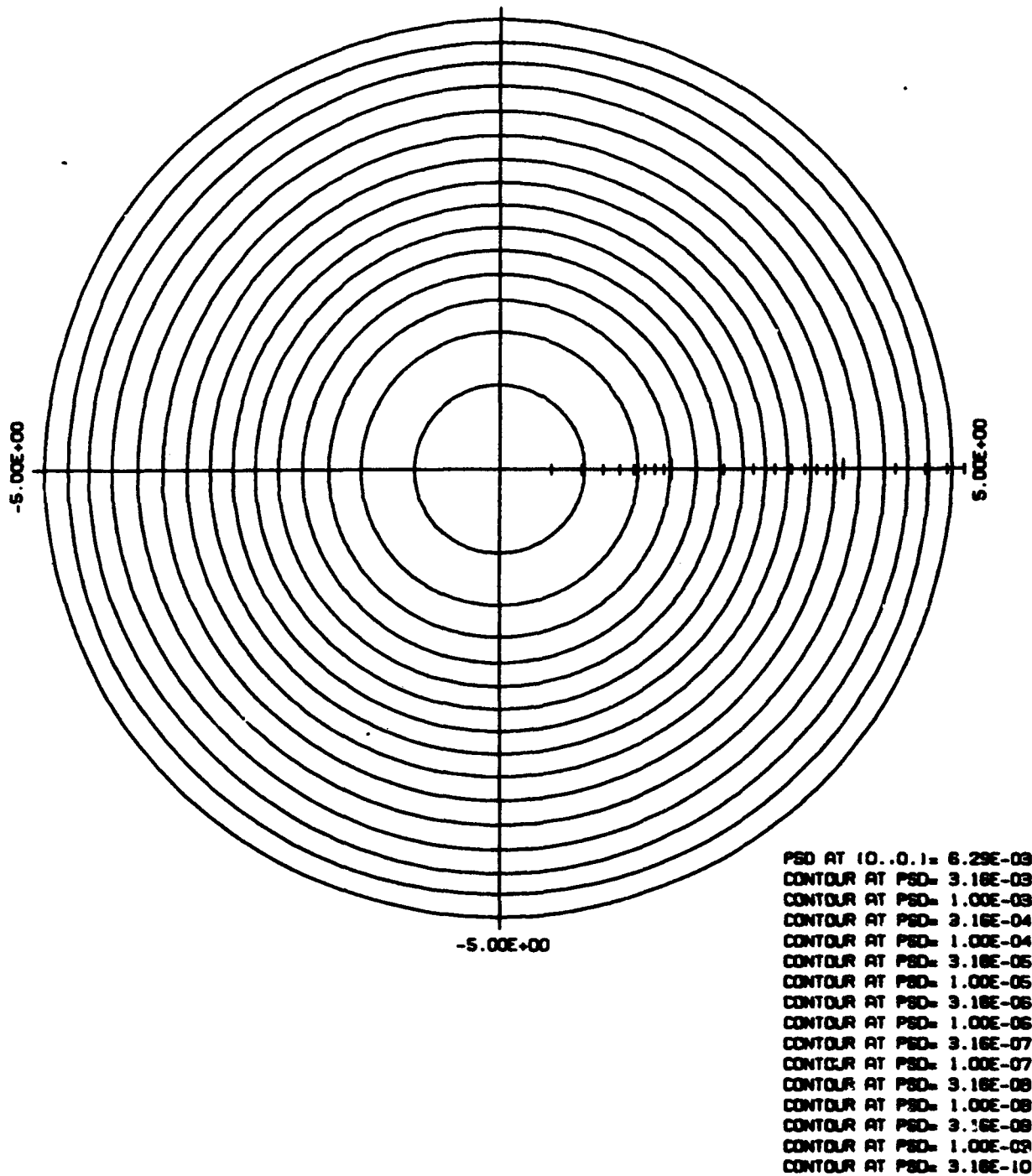


Figure 13. Same as Figure 4, except  $L_C = 84$  km and 2-D slope = -3.67

LC= 3.20E+01 SIGMA=2.00E-01 SLOPE OF PRED=0.97  
 R= 3.71E-03 WEIGHT LOWEST PRED BY 1.00E+02  
 MA ORDER 3 X 3 NA ORDER 7 X 7  
 MIN. FRE. #1/INCR= 3.71E-05 MAX. FRE. #1/INCR= 1.00E+01

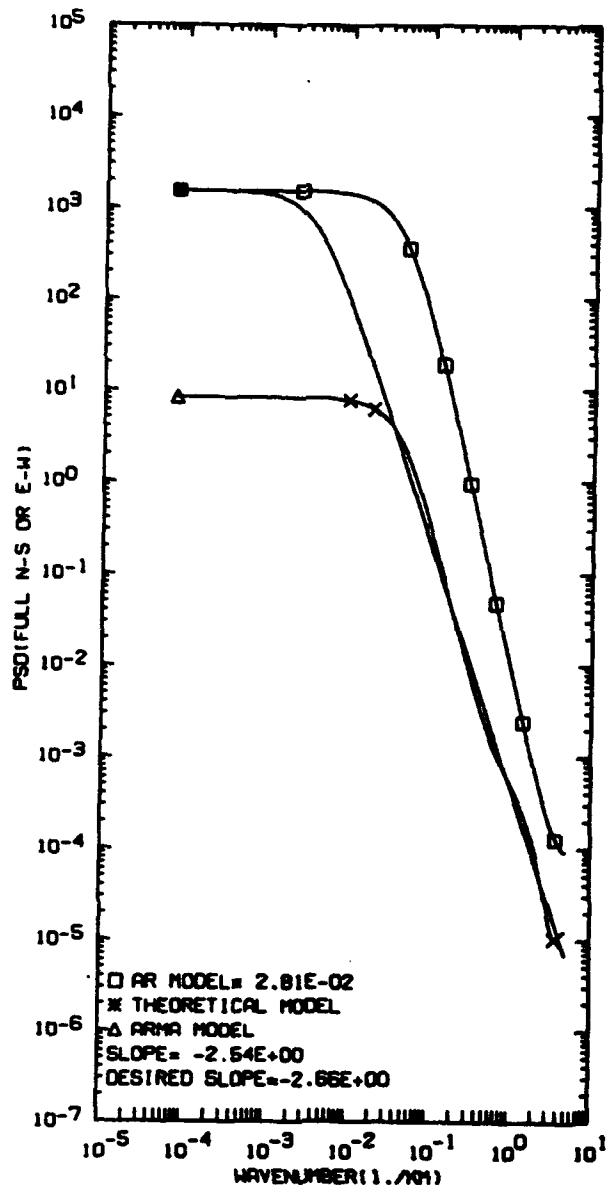


Figure 14. Same as Figure 1, except number of frequencies, N = 1024

LC= 3.50E-01 SIGMA= 2.00E-01 SLOPE OF PSD= 0.57  
 R= 3.71E-08 WEIGHT LOWEST FREQ BY 1.00E+02  
 AR ORDER 13 X 13 MA ORDER 25 X 25  
 MIN. FREQ. = 1/1024 = 9.77E-05 HZ NOISE NOISE4 AND ON= 1.00E-01

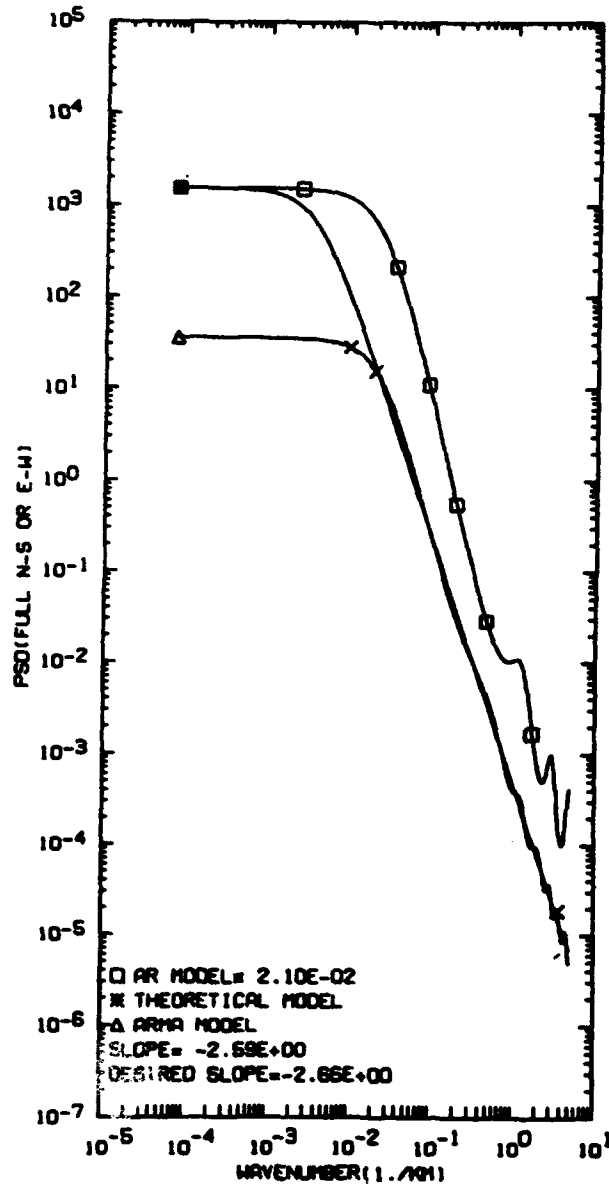


Figure 15. Same as Figure 14, except the order of AR coefficients = 13 x 13. Order of MA coefficients = 25 x 25, N = 1024.

## 5. SIMULATION - PROCEDURE

To simulate sets of two-dimensional Gaussian correlated data from the model filters described above, we start out with a sheet of pseudo-random numbers having a standard deviation  $\sigma = 1$ . The square  $N \times M$  sheet ( $N = M = 1300$ ) is somewhat larger than the sheet we wish to simulate, say an extra 138 values on each side. The extra points allow iterative relaxation. Figure 16 depicts the  $1300 \times 1300$  two-dimensional sheet of random numbers.

A problem ensues when we attempt to employ the full plane  $A(f_x, f_y)$  filter.  $A(f_x, f_y)$  is not a "computable" infinite impulse response filter. A "computable" filter can be applied directly to a sheet of numbers.  $A(f_x, f_y)$ , however, involves the solution of  $N^2$  linear equations in  $N^2$  unknowns. For  $N \sim 1000$ , the computational requirements become prohibitive. An approximate solution is therefore obtained as follows.

An initial "guess" for the solution of the  $N^2$  equations in  $N^2$  unknowns is made by summing the separate results of four quarter plane filters,  $A_{A1}(f_x, f_y)$ , applied to each corner of the same sheet of random numbers. Each of the quarter plane filters is "computable". In effect, computable means that the resulting  $N^2$  linear equations in  $N^2$  unknowns can be written as the solution of a triangular matrix equation. The four quarter plane filters are derived from the full plane filter coefficients as follows, where  $a(m, n)$  are the full plane AR filter coefficients and  $a1(m, n)$ ,  $a2(m, n)$ ,  $a3(m, n)$ , and  $a4(m, n)$  are the four quarter plane filter coefficients:

Let  $a1(m, n) = 0$  for  $m < 0$  or  $n < 0$

$a1(m, n) = 2a(m, n)$   $m = 0, n > 0$

$a1(m, n) = 2a(m, n)$   $m > 0, n = 0$

$a1(m, n) = 4a(m, n)$   $m > 0, n > 0$

Let  $a2(m, n) = 0$  for  $m > 0$  or  $n < 0$

$a2(m, n) = 2a(m, n)$   $m = 0, n > 0$

$a2(m, n) = 2a(m, n)$   $m < 0, n = 0$

$a2(m, n) = 4a(m, n)$   $m < 0, n > 0$

Let  $a3(m, n) = 0$  for  $m < 0$  or  $n > 0$

$a3(m, n) = 2a(m, n)$   $m = 0, n < 0$

$a3(m, n) = 2a(m, n)$   $m > 0, n = 0$

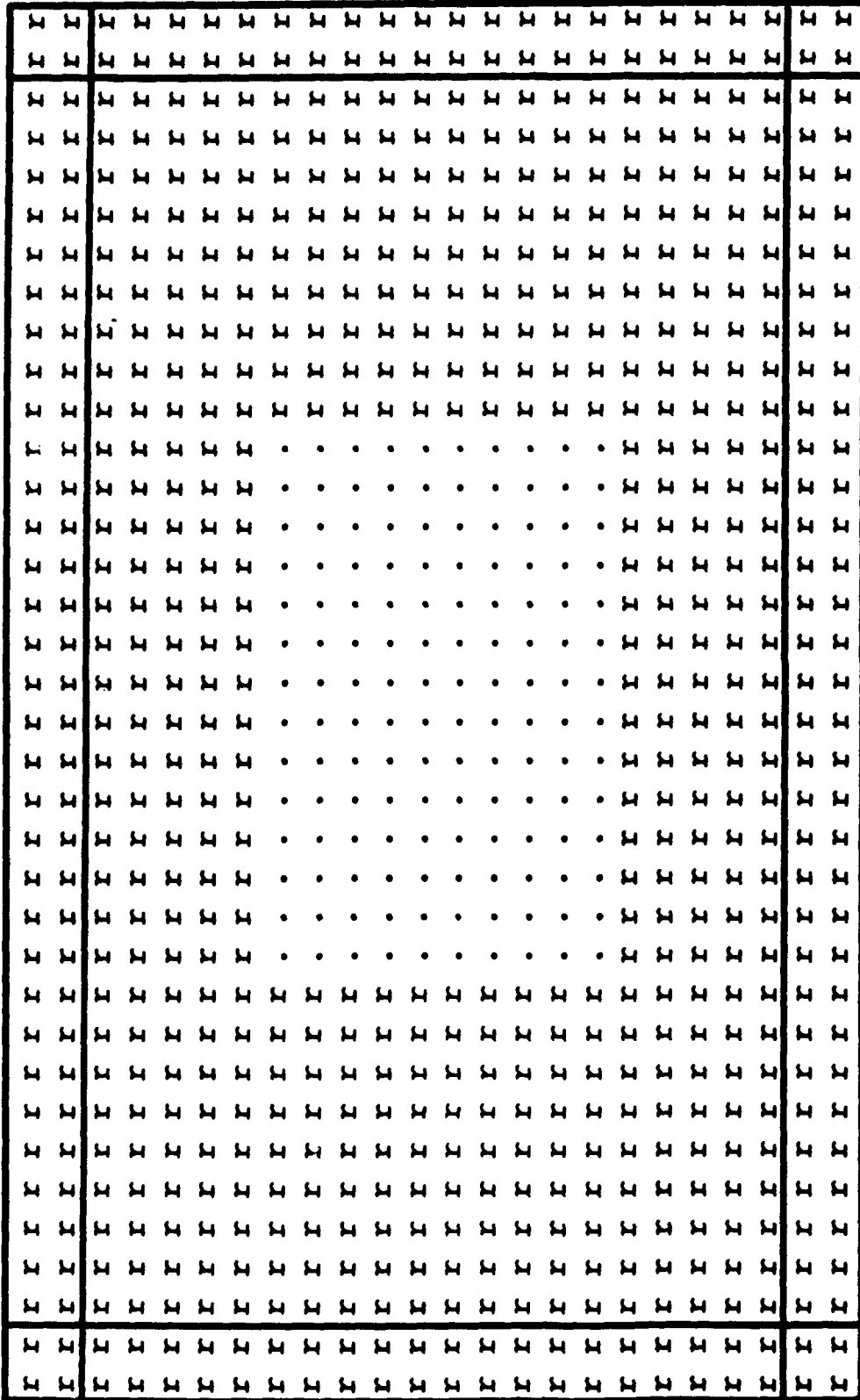
$a3(m, n) = 4a(m, n)$   $m > 0, n < 0$

Let  $a4(m, n) = 0$  for  $m > 0$  or  $n > 0$

$a4(m, n) = 2a(m, n)$   $m = 0, n < 0$

$a4(m, n) = 2a(m, n)$   $m < 0, n = 0$

$a4(m, n) = 4a(m, n)$   $m < 0, n < 0$



Sheet of 1300 x 1300 random numbers ( $r$ ) = 1,690,000 points total.  
 Extra points have edge width = 138 points for 641,424 extra edge points.  
 Internal (simulation values) = 1024 x 1024 = 1,048,576 points.  
 A certain width of boarder points remain unchanged after filtering .

Figure 16. Pictorial representation of two-dimensional sheet of Gaussian random numbers

These relationships are schematically illustrated in Figure 17. The principal reason for employing this initialization procedure is that it seems to allow the iteration scheme described below to converge faster to the actual solution. In general, iteration schemes that attempt to simulate filtered data converge inversely with the power spectral density as a function of frequency. Since the greatest power occurs at the lowest frequencies, we therefore wish to devise an initialization procedure that enables the low frequency behavior of the simulation to follow the low frequency behavior of the AR filter. This is accomplished with near circular symmetry by summing the results of the four quarter plane filters. Figures 18, 19, and 20 illustrate the method for applying the quarter plane filter. Figure 18 depicts the starting condition for a 2 x 2 quarter plane AR example (derived as implied above from a 3 x 3 full plane AR model; that is, 0 q.p. = (0 f.p. + 1) / 2). The procedure is iterative and starts in the upper right corner. The arrows indicate that the filter is moved column-wise to the left. At the left edge of the sheet, the filter is brought back to the right and dropped one row. Figure 19 shows an intermediate stage in the first corner process. It illustrates that points within and to the right of the filter have been processed, while points in the adjacent first row to the left of the filter region also have been processed. In this particular iteration, the point at the extreme left-bottom of the 2 x 2 filter region contains the original random number but gets replaced by the 2 x 2 AR filtered value. Note that points in the one-point-wide border remain unprocessed. Figure 20 illustrates the starting condition for the second pass at the upper left corner. Here the filter is moved to the right and then down. The extreme right-bottom point in the filter region contains the original random number but gets replaced by the 2 x 2 filtered value. After four such passes, (one pass starting from each corner and each pass using the same original random numbers) the results are summed. The following analysis indicates why the four-quarter-plane solution provides a good approximation of the low frequency behavior.

We have,

$$\frac{1}{A_A(f_x, f_y)} = \frac{1}{A_{A1}(f_x, f_y)} + \frac{1}{A_{A2}(f_x, f_y)} + \frac{1}{A_{A3}(f_x, f_y)} + \frac{1}{A_{A4}(f_x, f_y)}$$

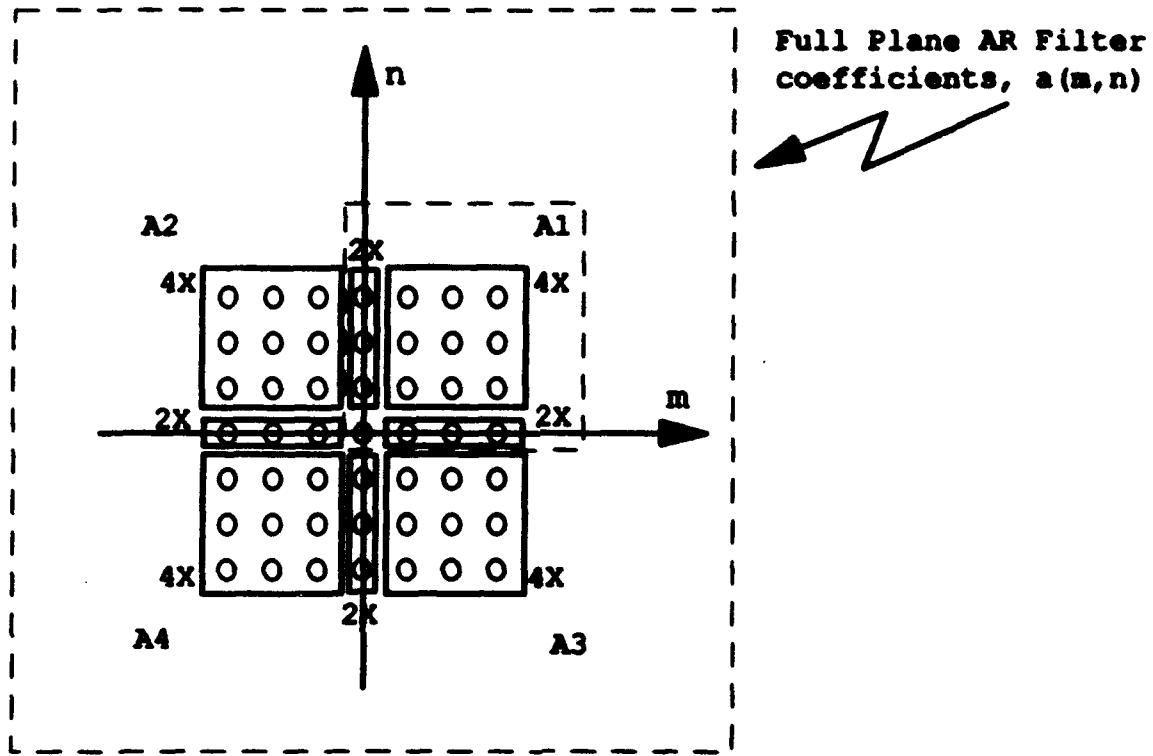
where  $A_A(f_x, f_y)$  is the AR filter associated with the sum of the four quarter plane filters and  $A_{Ai}(f_x, f_y)$  is the AR filter associated with the  $i^{\text{th}}$  quarter plane filter.

Using the identity,  $e^{-ix} = \cos(x) - i \sin(x)$  and setting  $N = M$  and  $T_1 = T_2$ , we have,

$$\frac{1}{A_{Ai}(f_x, f_y)} = \frac{1}{\sum_{m=-M}^M \sum_{n=-N}^N a_i(m, n) \left\{ \cos[2\pi T_1(mf_x + nf_y)] - i \sin[2\pi T_1(mf_x + nf_y)] \right\}}$$

and as  $f_x \rightarrow 0$  and  $f_y \rightarrow 0$

$$\frac{1}{A_{Ai}(f_x \rightarrow 0, f_y \rightarrow 0)} = \frac{1}{\sum_{m=-M}^M \sum_{n=-N}^N a_i(m, n) \cos(2\pi T_1 m f_x) \cos(2\pi T_1 n f_y)}$$



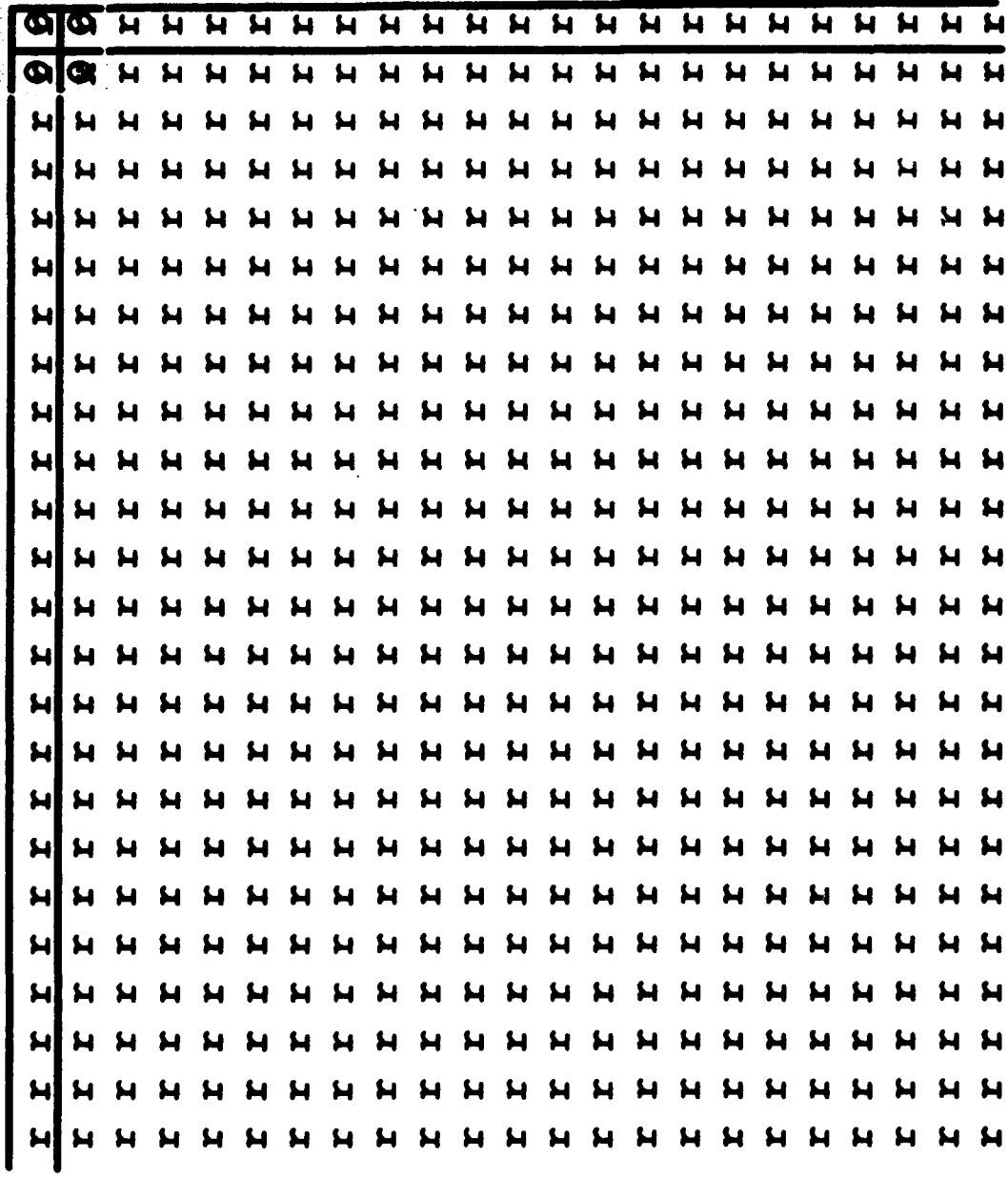
Full Plane filter coefficient symmetries

$$a(m,n) = a(-m,n) = a(m,-n) = a(-m,-n) = \\ = a(n,m) = a(-n,m) = a(n,-m) = a(-n,-m)$$

4 quarter plane filter symmetries as derived for each of the four corners.

$$a_1(n,m) = a_4(-n,m) \\ a_2(-n,m) = a_3(m,-n) = a_1(n,m)$$

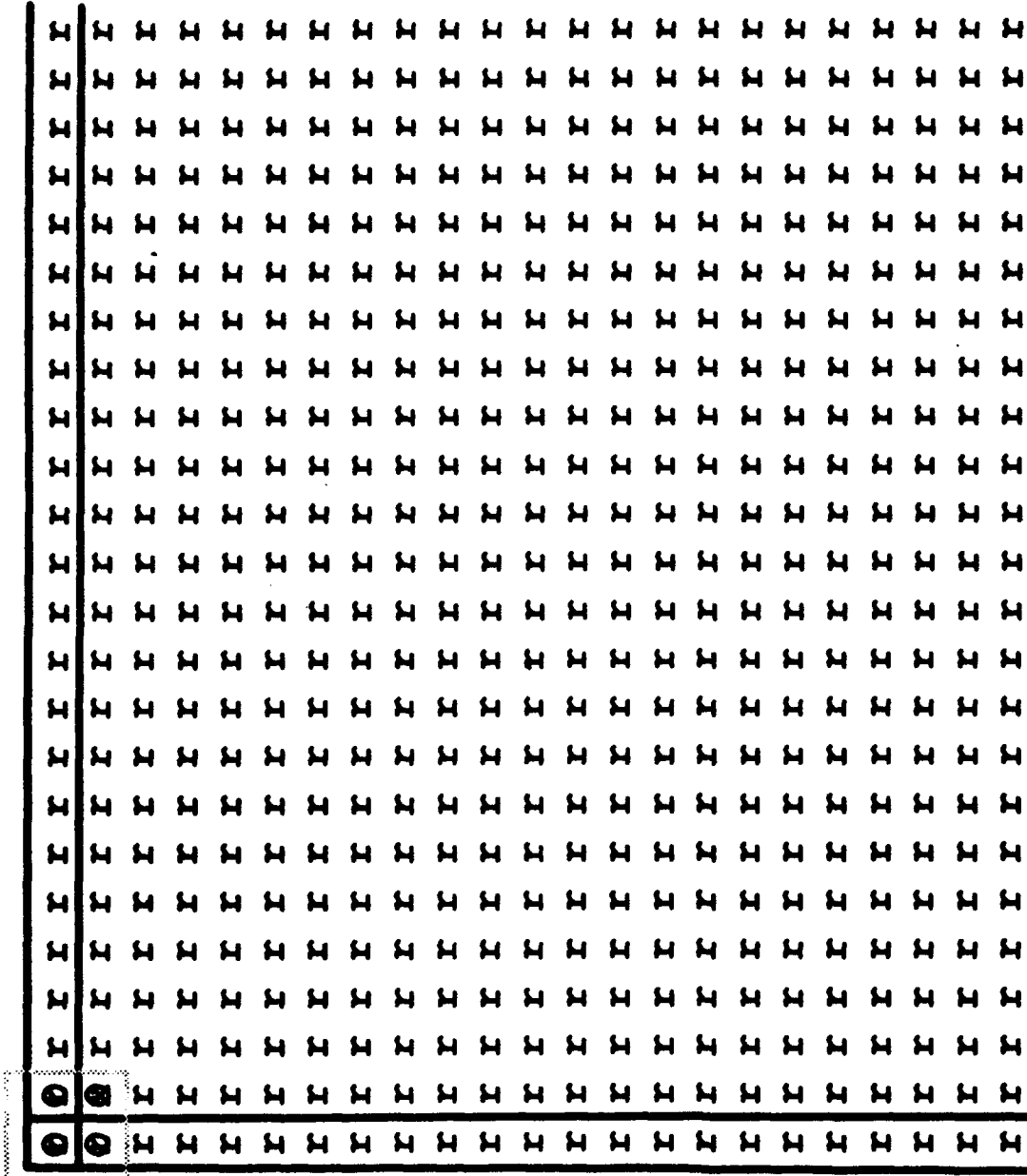
Figure 17. Diagram of symmetrical relationships of four quarter-plane AR filters to each other and to the AR full plane region of support



Quarter Plane 2 x 2 AR filter example. Procedure is iterative. Start from upper right corner. Moving to the left, operate on the random numbers. At end of each row, replace numbers by the iterates and move the filter back to the right edge and down one row -- repeat to end of sheet. One point wide in border remain unfiltered. r = random number. x = replacement value. O = filter coefficient.

Figure 18. Diagram of starting condition for application of first quarter plane AR filter. Example depicted for 2 x 2 AR quarter plane region of support





Same AR quarter plane 2 x 2 filter and same random numbers as before, but start from upper left. Proceed to right edge of sheet. At right edge replace random numbers by iterates, then return to left edge and step down one row -- repeat to end of sheet. Repeat entire process from lower left corner. Repeat again from lower right corner. Complete the initialization by adding the four quarter plane iterates.

Figure 20. Diagram of starting condition for application of second quarter plane AR filter. Depicted for same 2 x 2 AR quarter plane region of support

and, noting that  $a_1(m,n) = a_2(-m,n) = a_3(-m,-n) = a_4(m,-n)$ ,

$$\begin{aligned}
 A_A &= \frac{1}{\sum_{m=0}^M \sum_{n=0}^N a_1(m,n) \cos(2\pi T_1 m f_x) \cos(2\pi T_1 n f_y)} + \frac{1}{\sum_{m=0}^M \sum_{n=0}^N a_1(m,n) \cos(-2\pi T_1 m f_x) \cos(-2\pi T_1 n f_y)} \\
 &+ \frac{1}{\sum_{m=0}^M \sum_{n=0}^N a_1(m,n) \cos(-2\pi T_1 m f_x) \cos(2\pi T_1 n f_y)} + \frac{1}{\sum_{m=0}^M \sum_{n=0}^N a_1(m,n) \cos(2\pi T_1 m f_x) \cos(-2\pi T_1 n f_y)} \\
 &= \frac{4}{\sum_{m=0}^M \sum_{n=0}^N a_1(m,n) \cos[2\pi T_1 (m f_x + n f_y)]} \\
 &= \frac{4}{\sum_{m=0}^M \sum_{n=0}^N a_1(m,n) [\cos(2\pi m f_x T_1) \cos(2\pi n f_y T_1) - \sin(2\pi m f_x T_1) \sin(2\pi n f_y T_1)]} \\
 &= \frac{4}{\sum_{m=0}^M \sum_{n=0}^N a_1(m,n) [\cos(2\pi m f_x T_1) \cos(2\pi n f_y T_1)]}
 \end{aligned}$$

where again, we have ignored the sine terms. Recalling the symmetries of the  $a_1(m,n)$  coefficients, we find,

$$\begin{aligned}
 4A_A(f_x, f_y) &= 4 \sum_{m=1}^M \sum_{n=1}^N a(m,n) \cos(2\pi f_x m T_1) \cos(2\pi f_y n T_1) \\
 &+ 2 \sum_{n=1}^N a(0,n) \cos(2\pi f_y n T_1) + 2 \sum_{m=1}^M a(m,0) \cos(2\pi f_x m T_1) + a(0,0)
 \end{aligned}$$

and arrive at the approximation,  $\frac{1}{A_A(f_x, f_y)} \sim \frac{4}{A(f_x, f_y)}$  as  $f_x \rightarrow 0$  and  $f_y \rightarrow 0$ . It is unclear why the sum of the filters

performs better than the average. A more complete description of this process for the four quarter plane filters is provided in the appendix.

The four-quarter-plane procedure provides an initial guess for the correct data array. Subsequently, this initial guess is used as input to the full plane process. Following the four-quarter-plane initialization, the procedure continues by iteratively updating and correcting the spatial data set in the following way. At a point in the array  $(x,y)$  we sum the products of all neighboring points within the region of support and their corresponding full plane coefficients. To this sum is added the original  $(x,y)$  random number  $\epsilon(x,y)$ ; the result replacing the latest  $(x,y)$  value. This procedure continues for each point  $(x,y)$  in the array. Array substitutions are made in the same order as taken for the four quarter plane filters. To vector optimize for the Convex computer, elements in the lower row of the filter region were not replaced until all columns of that row were processed. The optimization process decreased computer run times significantly. One

set of substitutions (a set being defined by the same and every path taken by the four passes as previously defined for the four quarter plane passes - one pass per corner) constitutes one total iteration in this stage of the procedure.

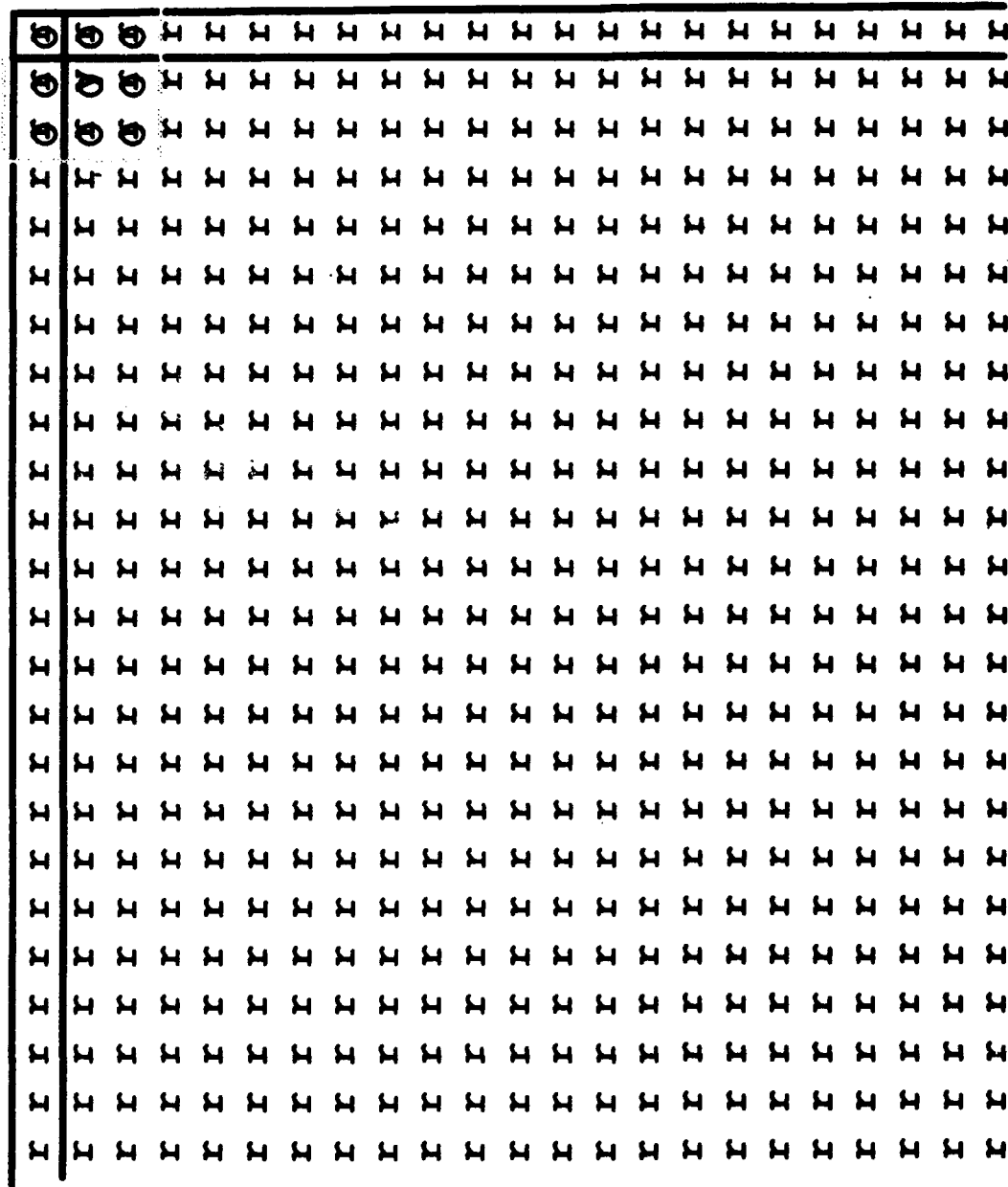
Figures 21 and 22 illustrate application of the full plane autoregressive filter  $A(f_x, f_y)$  using multiple predictor-corrector iterations. Figure 21 shows the starting condition for a  $3 \times 3$  full plane AR example. The plane is initialized by the final (summed) values of the quarter plane AR process as described above. As before, the procedure is iterative and starts in the upper right corner. Also, as described before, points in a one-point-wide border remain unprocessed. Figure 22 shows an intermediate stage in the first corner process. It illustrates that points above the center point and points to the right in the row adjacent to the center point of the filter have been processed. In this iteration, the center point of the  $3 \times 3$  filter region contains the original random number but gets replaced by the  $3 \times 3$  full plane AR filtered value. Four such passes, one starting from each corner, are performed. Unlike the quarter plane initialization process, each subsequent pass is performed on the numerical results of the preceding pass. Consequently, no summing is performed. We emphasize, however, that every iteration begins with a center value equal to the original random number, which gets replaced by the full plane AR filtered value. As discussed earlier, it is necessary to cycle through the full plane AR procedure several times to achieve a satisfactory estimate of the set of 1300 linear equations in 1300 unknowns. In general, we find that 20 cycles provides reasonable power spectral densities that parallel the "theoretical" PSD's.

Figure 23 illustrates application of the final moving average filter  $B(f_x, f_y)$ . The MA process is a mapping procedure that is performed only once on the sheet containing the final numerical results of the full plane process. As before, we start from the upper right corner and proceed left and down. Actually we could start and end anywhere since the process simply maps the center points of the  $7 \times 7$  MA full plane region to points co-located on a separate sheet.

## 6. ARMA SIMULATIONS - RESULTS AND DISCUSSION

In the above procedure we discussed a method for generating simulated two-dimensional correlated data by applying two-dimensional ARMA filters to Gaussian random noise. We now examine several simulated data sets for fidelity to the original or "theoretical" power spectral density specifications.

Figure 24 shows four logarithmic plots of two-dimensional power spectral density (PSD) versus logarithmic spatial frequency plotted along a diagonal axis. As before, the curve marked by an asterisk (\*) is the desired or "theoretical" PSD. The curve marked by open squares ( $\square$ ) represents the PSD of the full plane auto-regressive [AR] predictor model. The curve marked by an open triangle ( $\Delta$ ) at the first frequency represents the PSD of the full ARMA predictor model (which is to say, the [AR] model corrected by the moving average [MA] model). Finally, the curve marked by an X is a two-dimensional periodogram derived from two-dimensional simulated data. The  $1024 \times 1024$  simulated data set was derived from an original set of  $1300 \times 1300$  random numbers. Figure 24 is calculated for a "theoretical" 2-D slope of  $-8/3$  and correlation length  $L_c = 32$  km. The region of support for the full plane AR model is of order  $3 \times 3$  and the region of support for the full plane MA model is of order  $7 \times 7$ .



Full Plane 3 x 3 AR filter. Procedure is iterative. Start from upper right corner. Operate on initial predictors. Use original random numbers for each center point. Replace center numbers by the iterate and move filter to the left. At left edge of sheet, move filter back to the right edge and down one row. — Repeat to end of sheet.

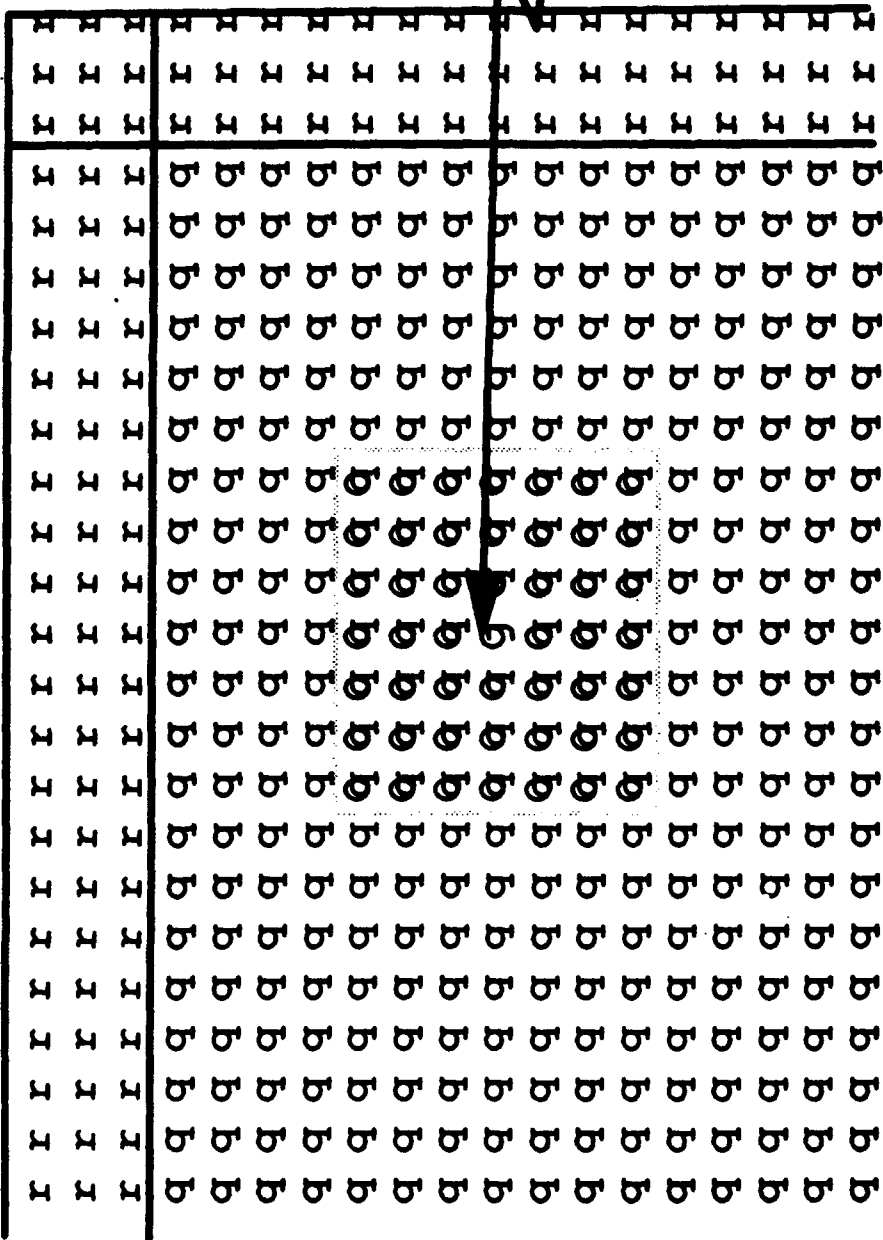
Figure 21. Diagram of starting condition for application of first full plane AR filter. Example depicted for 3 x 3 AR full plane region of support



Full Plane MA Filter. This is a mapping procedure. Start from upper right corner. Operate on final full plane AR predictor values. Map MA center numbers to new sheet. Move MA filter to left.

At left edge of sheet, move filter back to right edge and down one row. -- Repeat to end of sheet.

q = AR full plane predictor.  
j = MA full plane mapped value.



Operate on final full plane AR predictors. Map to new sheet. Figure shows 7 x 7 filter. Perform only once.

Figure 23. Diagram of intermediate step in processing the full plane moving average (MA) filter. Region of support represents a 7 x 7 order filter. Filter operates on final full plane AR values. MA filter maps center point to new sheet

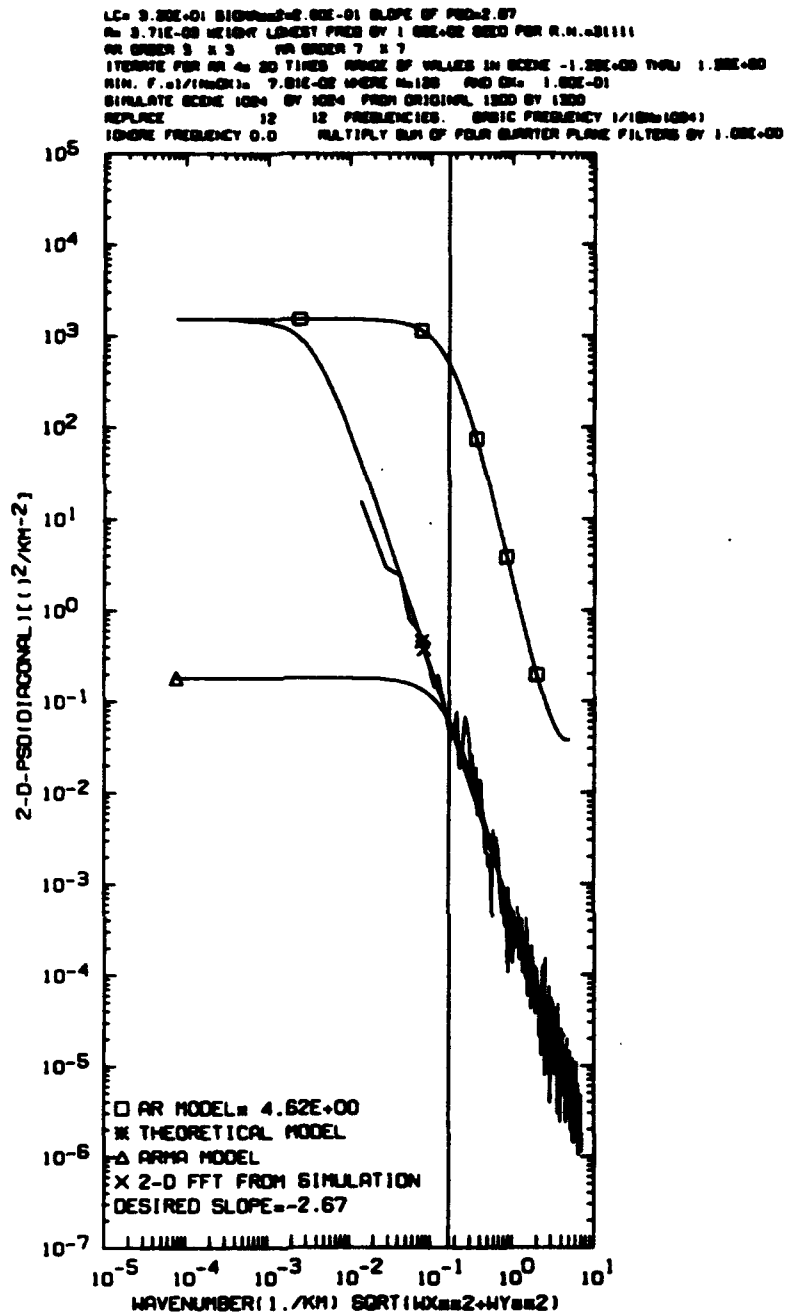


Figure 24. Log-log plot of two-dimensional power spectral density (PSD) versus spatial frequency plotted along a diagonal. Curve marked by an asterisk (\*) is the desired or "theoretical" PSD. Curve marked by open squares (□) represents the PSD of the full plane auto-regressive [AR] predictor model multiplied by the factor indicated on the plot. Curve marked by an open triangle (△) at the first frequency represents the PSD of the full ARMA predictor model (which is to say, the AR model corrected by the moving average [MA] model). Curve marked by an X is the 2-D periodogram derived from the 2-D simulation. The 1024 x 1024 simulated data set was derived from an original set of 1300 x 1300 random numbers (see text for discussion of DFT low frequency replacement). The "theoretical" 2-D slope is -2.67 and the correlation length  $L_c = 32$  km. The order of the AR coefficients = 3 x 3. Order of the MA coefficients = 7 x 7

As noted, the 2-D FFT periodogram corresponding to Figure 24 was calculated from the 1024 x 1024 simulated data array. However, since a goal of this effort was to minimize the computational burden, the minimum frequency that was adequately modeled by the 3 x 3 AR and 7 x 7 MA processes occurred at a minimum frequency of  $f_{\min} = \frac{1}{N\Delta x} = \frac{1}{128 \times 0.1} = 0.078 \text{ km}^{-1}$ . To expand the usable frequency range and lower the minimum simulated frequency to  $f_{\min} = \frac{1}{1024 \times 0.1} = 0.0098 \text{ km}^{-1}$  the following procedure was performed. At each frequency below  $0.078 \text{ km}^{-1}$ , the power (as determined by the 2-D FFT periodogram) was subtracted from the 1024 x 1024 simulated data array. A short 12 x 12 discrete Fourier transform, DFT, procedure was then performed to replace the simulated power from  $0.0098 \text{ km}^{-1}$  to  $0.078 \text{ km}^{-1}$ . A detailed description of the procedure may be found in the appendix. Agreement between the 2-D FFT periodogram and the ARMA model is good to  $0.078 \text{ km}^{-1}$ . With the addition of the DFT replacement procedure, agreement with the "theoretical" PSD curve is good over the entire frequency range,  $0.0098 \text{ km}^{-1}$  to  $5 \text{ km}^{-1}$ .

One may also examine the simulation by comparing the "theoretical" one-dimensional power spectral density of the two-dimensional data to one-dimensional equivalents of the simulated data. Figure 25 shows three logarithmic plots of one-dimensional power spectral density (PSD) versus logarithmic spatial frequency plotted along a major axis. The curve marked by an asterisk (\*) is the desired or "theoretical" 1-D PSD. The curve marked by an open circle (o) at the first frequency represents the 1-D PSD derived by integrating the 2-D PSD ARMA model. Finally, the curve marked by an X at the first frequency represents a one-dimensional autoregressive PSD model derived from the simulated 2-D data. The latter is accomplished by treating all rows and columns as 1-D data and finding the corresponding AR model. The parameters are the same as used in Figure 24 with the 2-D -8/3 slope becoming a 1-D slope of -5/3. Figure 25 shows that the 1-D power spectral density curve as derived by integrating the 2-D ARMA model is faithful to the "theoretical" model. Of course the curve rolls off as it approaches its lower limit. Also, the 1-D AR power spectral density curve follows the "theoretical" to much lower frequencies. The slight overshoot of the AR-PSD model seems to be due to the difficulty in approximating the PSD at low frequencies using an AR model of limited extent.

We may also examine the one-dimensional FFT periodogram derived from the simulated two-dimensional data set. Figure 26 shows the same curves as Figure 25, except that the curve marked by an X is the one-dimensional power spectral density derived by finding the FFT of all rows and columns. Again, good agreement obtains between the "theoretical" and the 1-D periodogram. Of course, at the expense of computer time, better and better agreement would obtain (especially near the "rollover" frequency) as the number of AR iterations increase.

Figures 27 and 28 show the same four two-dimensional PSD plots as Figure 24 except that Figure 27 is plotted for a slope of -3 and Figure 28 is plotted for a slope of -11/3. These cases show that the simulated data retains high fidelity to the "theoretical" 2-D PSD slope from -8/3 to -11/3.

```

LC= 3.20E-01 SIGMA=2.20E-01 SLOPE OF PSD=-1.67
R= 2.71E-03 HEIGHT LOWEST PSD BY 1.00E-02 GRID FOR R.N.=81111
AR ORDER 3 X 3 MA ORDER 7 X 7
ITERATE FOR AR 40 50 TIMES RANGE OF VALUES IN SCENE -1.00E-03 THRU 1.00E-03
WIN F=0.1/100000 7.01E-03 MORE NOISE AND SNR 1.00E-01
SIMULATE SCENE 1024 BY 1024 FROM ORIGINAL 1280 BY 1280
REPLACE SCENE 12 12 FREQUENCIES. BASIC FREQUENCY 1/1000000
IGNORE FREQUENCY 0.0

```

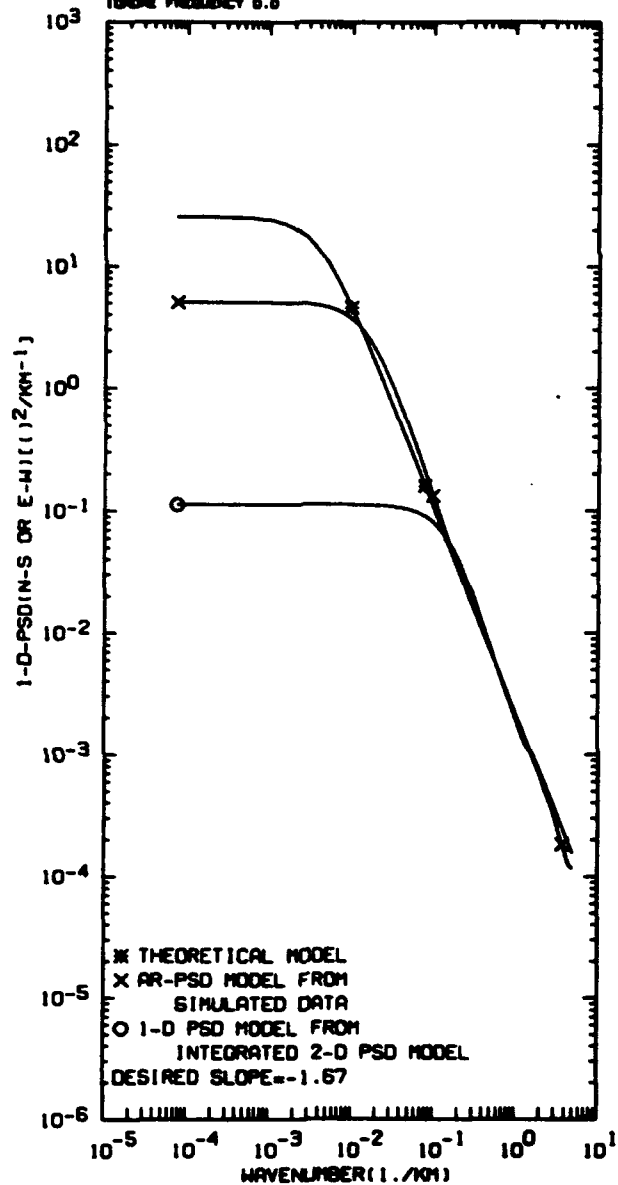


Figure 25. Log-log plot of one-dimensional power spectral density (PSD) versus spatial frequency plotted along a major axis. Curve marked by an asterisk (\*) is the desired or "theoretical" 1-D PSD. Curve marked by an open circle (o) at the first frequency represents the 1-D PSD derived by integrating the 2-D PSD ARMA model. Curve marked by an X at the first frequency represents an autoregressive PSD model derived from the simulated 2-D data (with DFT low frequency replacement). The 1024 x 1024 simulated data set was derived from an original set of 1300 x 1300 random numbers. The "theoretical" 1-D slope is -1.67 and the correlation length  $L_c = 32$  km. The order of the AR coefficients = 3 x 3. Order of the MA coefficients = 7 x 7

LC= 3.0E-01 SIGMA=2.0E-01 SLOPE OF PSD=-1.67  
 IN 3.71E-03 HEIGHT LOWEST FREQ OF 1.0E-02 USED FOR R.N.=01111  
 OR ORDER 3 X 3 OR ORDER 7 X 7  
 ITERATE FOR AN IN 20 TIMES RANGE OF VALUES IN SCENE -1 0E+00 MAX 1.0E+00  
 WITH F.0/ITERATE= 7.0E-02 MORE VALUE FOR MAX 1.0E-01  
 SIMULATE SCENE 1004 BY 1004 FROM ORIGINAL 1200 BY 1200  
 REPLACE 12 12 PERIODIC. BASIC PERIODIC 1/(1000000)  
 SCENE FREQUENCY 0.0

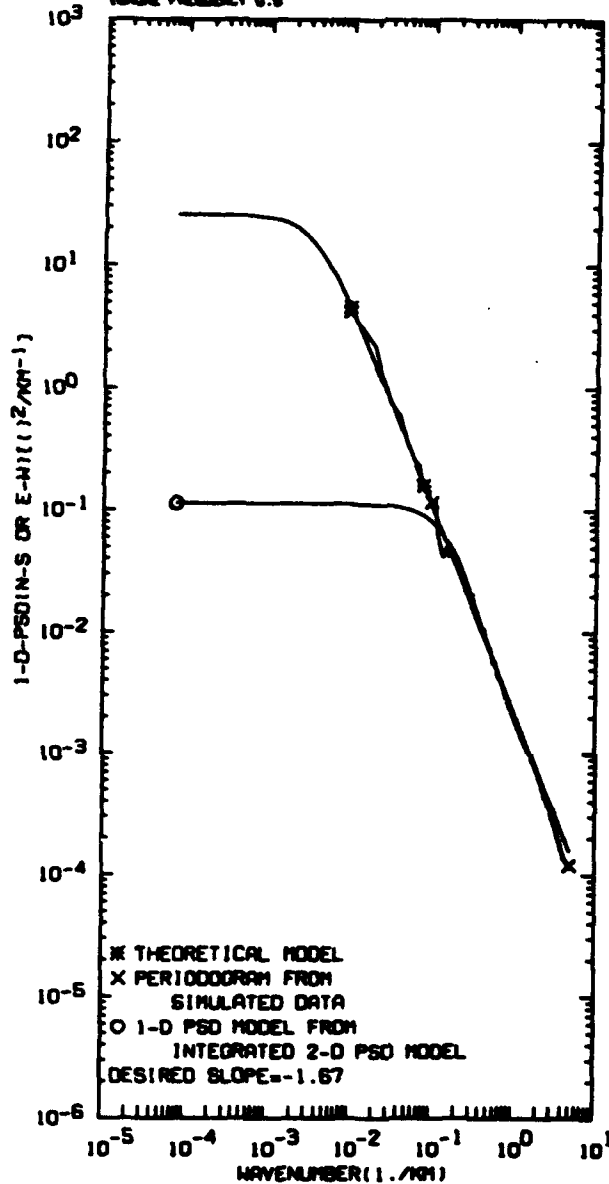


Figure 26. Log-log plot of one-dimensional power spectral density (PSD) versus spatial frequency plotted along a major axis. Curve marked by an asterisk (\*) is the desired or "theoretical" 1-D PSD. Curve marked by an open circle (o) at the first frequency represents the 1-D PSD derived by integrating the 2-D PSD ARMA model. Curve marked by X's represents the 1D periodogram derived from the rows and columns of the 2-D simulated data (with DFT low frequency replacement). The 1024 x 1024 simulated data set was derived from an original set of 1300 x 1300 random numbers. The "theoretical" 1-D slope is -1.67 and the correlation length  $L_c = 32$  km. The order of the AR coefficients = 3 x 3. Order of the MA coefficients = 7 x 7

LC= 3.20E+01 SIGMA=2.00E-01 SLOPE OF PSD=-3.00  
 A= 4.97E-08 HEIGHT LARGEST PRED BY 1.00E-02 GRID FOR R.N.=01111  
 AR ORDER 3 X 3 AR ORDER 7 X 7  
 ITERATE FOR AR 20 TIMES RANGE OF VALUES IN SCENE -1.00E+00 TO 1.10E+00  
 WIN. 7.01/10000 7.00E-02 WERE USED AND ON 1.00E-01  
 SIMULATE SCENE 1004 BY 1004 FROM ORIGINAL 1300 BY 1300  
 REPLACE 12 12 PREDICTIONS. BASIC FREQUENCY 1/1000004  
 IGNORE FREQUENCY 0.0 MULTIPLY SUM OF FOUR BLASTER PLANE FILTERS BY 1.00E+00

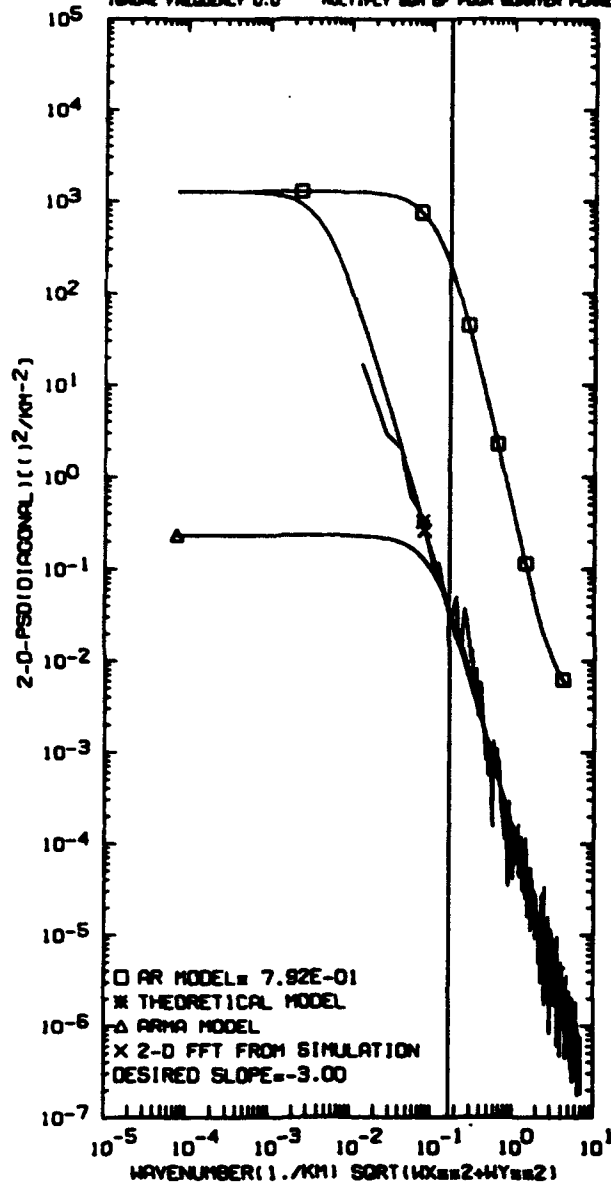


Figure 27. Same as Figure 24, except 2-D slope = -3.00

LC= 3.33E-04 SIGMA=2.00E-01 SLOPE OF PSD=3.67  
 R= 0.37E-00 HEIGHT LATEST PSD BY 1.00E-02 USED FOR R.N.=01111  
 AN ORDER 3 X 3 AN ORDER 7 X 7  
 ITORRE PER AN 20 TIMES RANGE OF VALUES IN SCENE -0.04E-04 TWRD 0.00E-04  
 MIN. F./MINUTE= 7.00E-02 MORE N.100 AND 0.0 1.00E-04  
 SIMULATE SCENE 1004 OF 1004 FROM ORIGINAL 1000 BY 1000  
 REPLACE 12 12 PROBENCIES. BASIC FREQUENCY 1/1000(1004)  
 HORIZE FREQUENCY 0.0 MULTIPLY OUT OF FOUR SLAYER PLANE FILTERS BY 1.00E-00

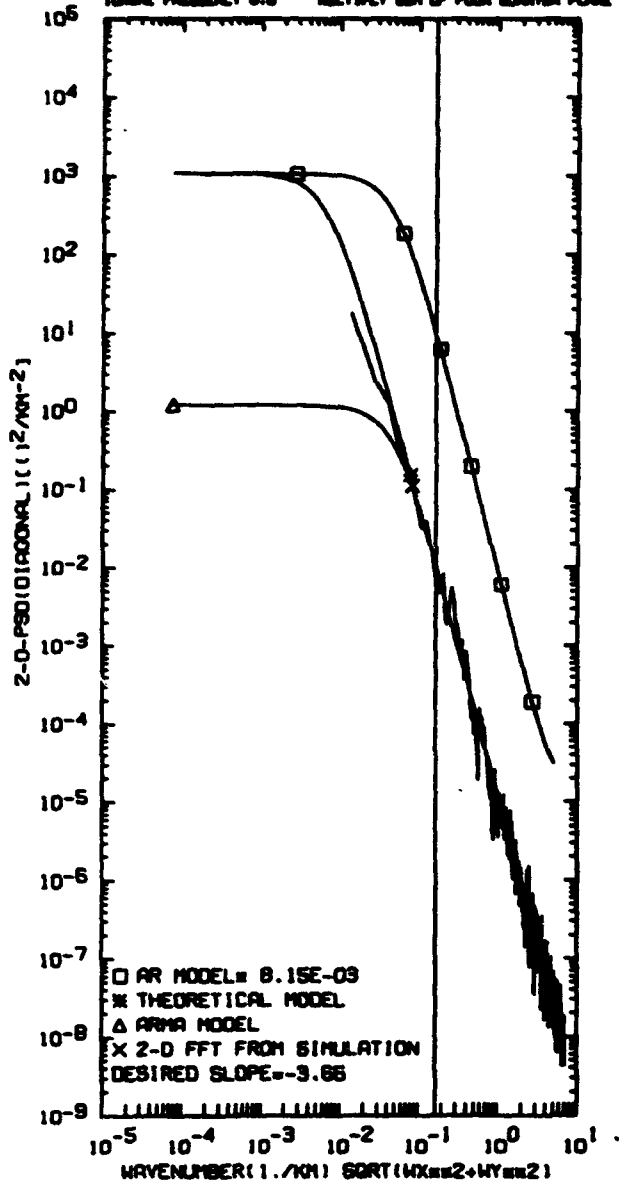


Figure 28. Same as Figure 24, except 2-D slope = -3.67

The curves presented in Figures 29, 30, and 31 repeat the plots of Figures 24, 27, and 28 except that  $L_c = 84$  km. Clearly the two-dimensional periodograms indicate good agreement with the "theoretical" PSD slopes for the entire spread of correlation lengths and spectral slopes.

The 2-D curves presented in Figure 32 repeat the plot of Figure 29 except Figure 32 is calculated for an AR order  $13 \times 13$ , MA order  $25 \times 25$ ,  $N = 1024$ , and with no low frequency replacement. Clearly, the AR and ARMA model curves match the "theoretical" PSD better; especially, the high order ARMA model matches the "theoretical" PSD to much lower frequencies. Also, the periodogram matches the "theoretical" PSD well. Not much improvement, however, was seen as the AR order increased above order  $13 \times 13$ . Again, the cost of increasing the ARMA model to high order is greatly increased computer time.

The 2-D curves presented in Figure 33 repeat the plots of Figure 29, except that the periodogram plot in this figure shows the effect of subtracting out the low frequency components from the  $1024 \times 1024$  ARMA simulated scene. The PSD falls abruptly by many orders of magnitude just below the 128 point "minimum" cutoff frequency. Figure 34 presents a two-dimensional gray scale  $102.4$  km  $\times$   $102.4$  km pictorial realization corresponding to Figure 33. The high-frequency-only structured data was constructed for  $L_c = 84$  km, 2-D slope =  $-8/3$ , spacing =  $100$  m, AR order =  $3 \times 3$ , and MA order =  $7 \times 7$  but with the low frequency components removed. The two figures show that the procedure described in the appendix is highly effective in removing the low frequency components, leaving only the ARMA high frequency components. Figure 35 repeats the curves presented in Figure 29, except that the periodogram shows only the added low frequency DFT replacement portion of the spectrum. Clearly, the  $12 \times 12$  replacement scheme, described in the appendix, is able to provide low frequency power components that match the "theoretical" PSD well.

For completeness, Figure 36 shows a finished two-dimensional gray scale pictorial realization of  $102.4 \times 102.4$  km ARMA simulated data with low frequency DFT replacement. The structured data were constructed for  $L_c = 84$  km, 2-D slope =  $-8/3$ , spacing =  $100$  m, AR order =  $3 \times 3$ , and MA order =  $7 \times 7$ . The model and calculated power spectral densities of this data were presented in Figure 29.

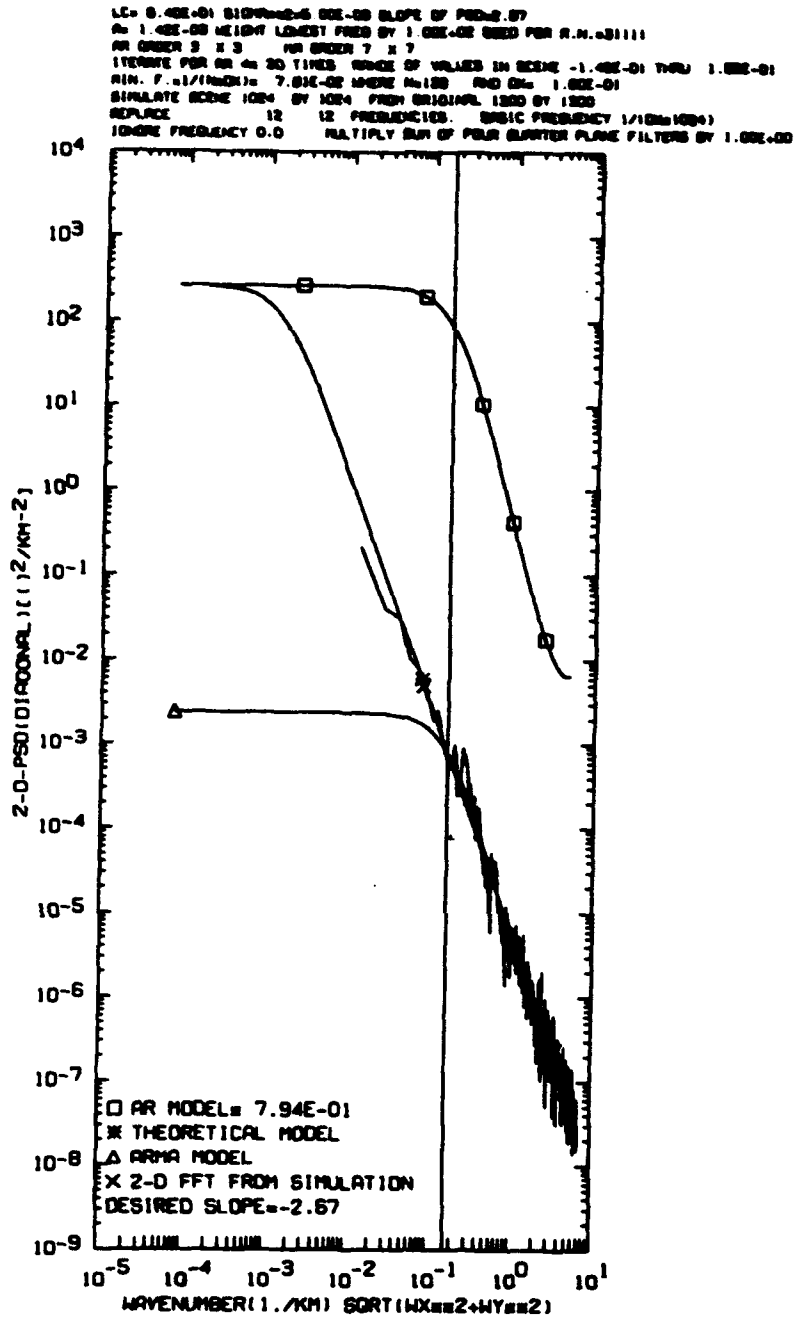


Figure 29. Log-log plot of two-dimensional power spectral density (PSD) versus spatial frequency plotted along a diagonal. Curve marked by an asterisk (\*) is the desired or "theoretical" PSD. Curve marked by open squares (□) represents the PSD of the full plane auto-regressive [AR] predictor model multiplied by the factor indicated on the plot. Curve marked by an open triangle (△) at the first frequency represents the PSD of the full ARMA predictor model (which is to say, the AR model corrected by the moving average [MA] model). Curve marked by an X is the 2-D periodogram derived from the 2-D simulation. The 1024 x 1024 simulated data set was derived from an original set of 1300 x 1300 random numbers (see text for discussion of DFT low frequency replacement). The "theoretical" 2-D slope is -2.67 and the correlation length  $L_c = 84$  km. The order of the AR coefficients = 3 x 3. Order of the MA coefficients = 7 x 7

LC= 0.40E-01 SIGMA=2=5.00E-03 SLOPE OF PSD=-3.00  
 R= 1.00E-03 HEIGHT LOWEST PRED BY 1.00E+02 USED FOR R.N.=01111  
 AR ORDER 3 X 3 AR ORDER 7 X 7  
 ITERATE FOR AN 20 TIMES RANGE OF VALUES IN SCENE -1.07E-01 THRU 1.18E-01  
 MIN. F.=(1/NOISE)= 7.81E-02 WHERE N=128 AND ON= 1.00E-01  
 SIMULATE SCENE 1024 BY 1024 FROM ORIGINAL 1300 BY 1300  
 REPLACE 12 12 FREQUENCIES. BASIC FREQUENCY 1/(10M\*10M)  
 IGNORE FREQUENCY 0.0 MULTIPLY SUM OF FOUR QUARTER PLANE FILTERS BY 1.00E+00

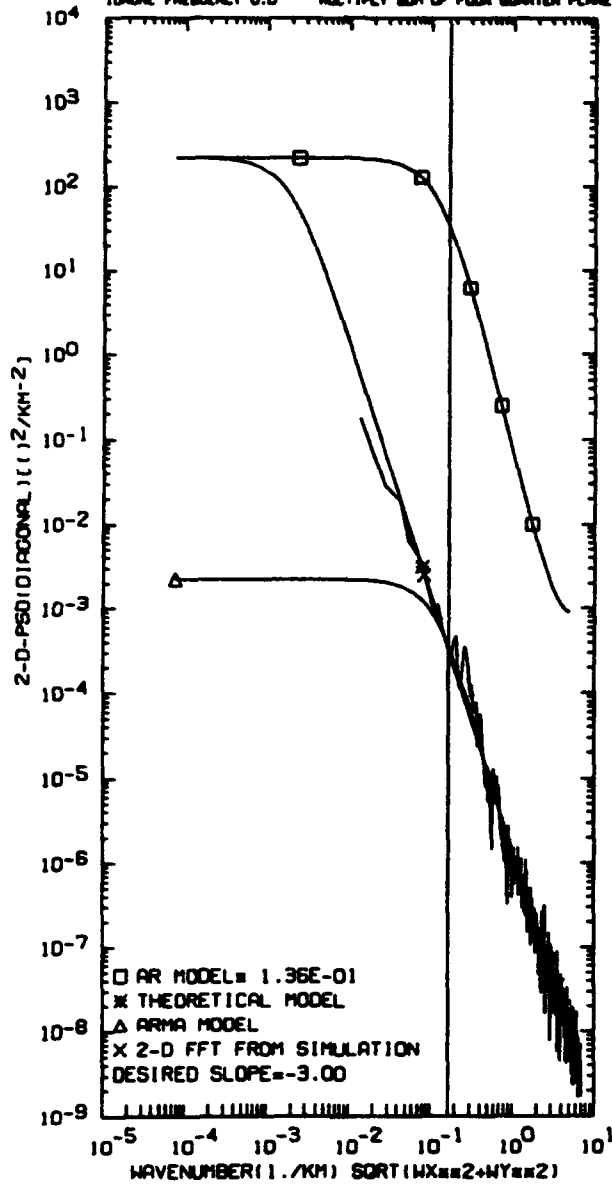


Figure 30. Same as Figure 29, except 2-D slope = -3

LC= 8.40E-01 SLOPE=2.5.00E-03 SLOPE OF PSD=-3.67  
 A= 2.00E-03 HEIGHT LOWEST FREQ BY 1.00E+02 USED FOR R.N.=3111  
 AR ORDER 3 X 3 MA ORDER 7 X 7  
 ITERATE FOR AR 40 20 TIMES RANGE OF VALUES IN SCENE -7.07E-02 THRU 7.00E-02  
 MIN. F.01/10000= 7.81E-02 WHERE N=128 AND Q= 1.00E-01  
 SIMULATE SCENE 1024 BY 1024 FROM ORIGINAL 1280 BY 1280  
 REPLACE 12 12 FREQUENCIES. BASIC FREQUENCY 1/10000041  
 IGNORE FREQUENCY 0.0 MULTIPLY SUM OF FOUR QUARTER PLANE FILTERS BY 1.00E+00

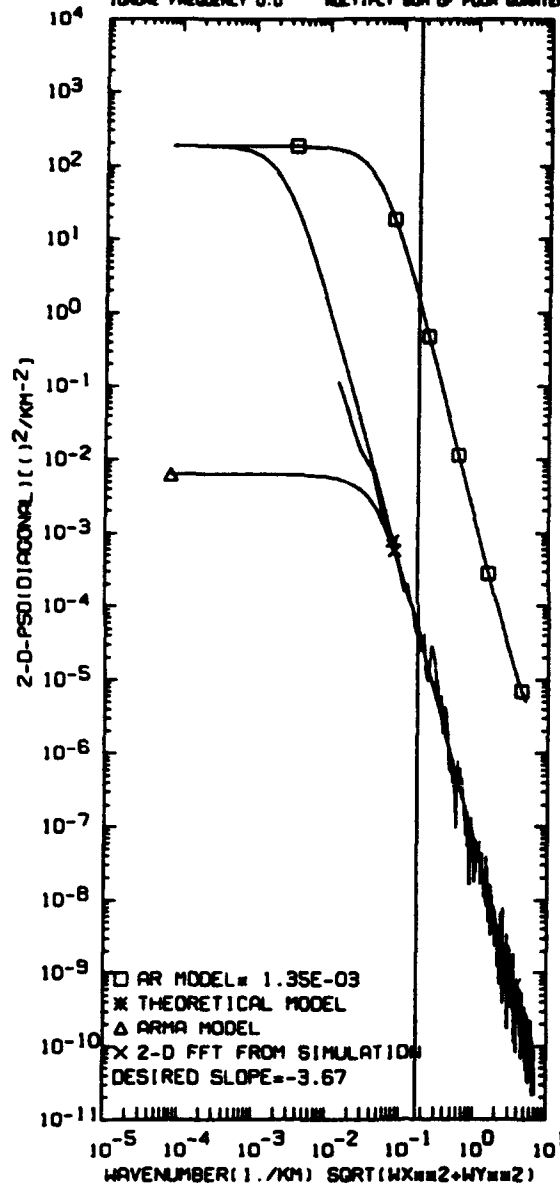


Figure 31. Same as Figure 29, except 2-D slope = -3.67

```

LC= 0.40E+01 SIGMA=2=5.00E-03 SLOPE OF PSD=2.67
A= 1.42E-03 HEIGHT LOWEST FREQ BY 1.00E+02 REED FOR R.N.=31111
AR ORDER 13 X 13 MA ORDER 25 X 25
ITERATE FOR AR A= 20 TIMES RANGE OF VALUES IN SCENE -8.00E-02 THRU 8.00E-02
MIN. F. 1/(10000)= 9.77E-03 WHERE M=1024 AND CM= 1.00E-01
SIMULATE SCENE 1024 BY 1024 FROM ORIGINAL 1300 BY 1300
REPLACE 0 0 FREQUENCIES BASIC FREQUENCY 1/(1000000)
IGNORE FREQUENCY 0.0 MULTIPLY SUM OF FOUR QUARTER PLANE FILTERS BY 1.00E+00

```

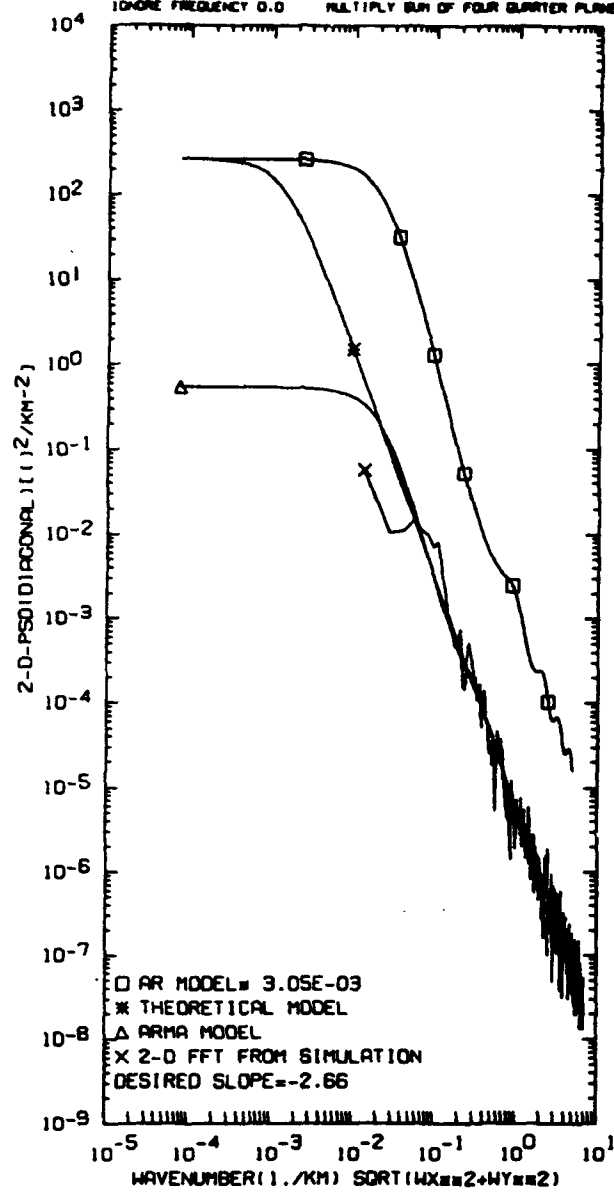


Figure 32. Same as Figure 29, except the order of the AR filter = 13 x 13 and the order of the MA filter = 25 x 25 (no DFT low frequency replacement values)

LC= 8.40E-01 SIGMA=2=5.00E-05 SLOPE OF PSD=-2.67  
 N= 1.42E-03 HEIGHT LOWEST PRED BY 1.00E-02 USED FOR R.N.=31111  
 AR ORDER 3 X 3 MA ORDER 7 X 7  
 ITERATE FOR AR N= 20 TIMES RANGE OF VALUES IN SCENE -8.57E-02 THRU 7.18E-02  
 RIN. F.01/(INCR)= 7.81E-02 WHERE N=128 AND OR= 1.00E-01  
 SIMULATE SCENE 1024 BY 1024 FROM ORIGINAL 1300 BY 1300  
 REPLACE 12 12 FREQUENCIES. BASIC FREQUENCY 1/(10\*1024)  
 IGNORE FREQUENCY 0.0

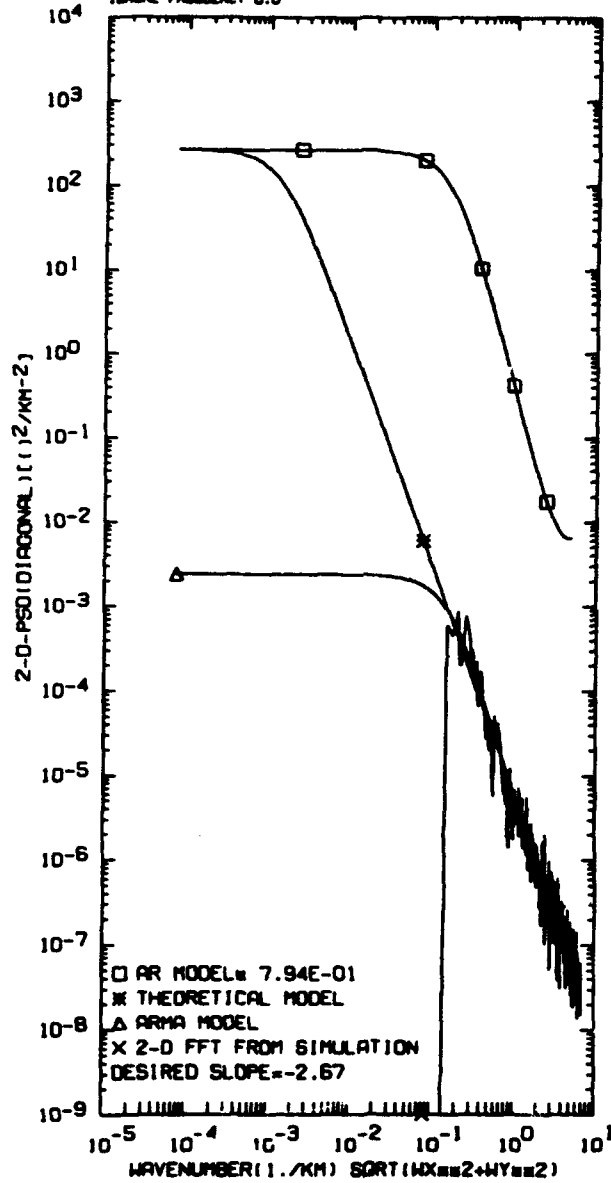


Figure 33. Same as Figure 29, except the low frequency power has been subtracted from the 1024 x 1024 simulated data

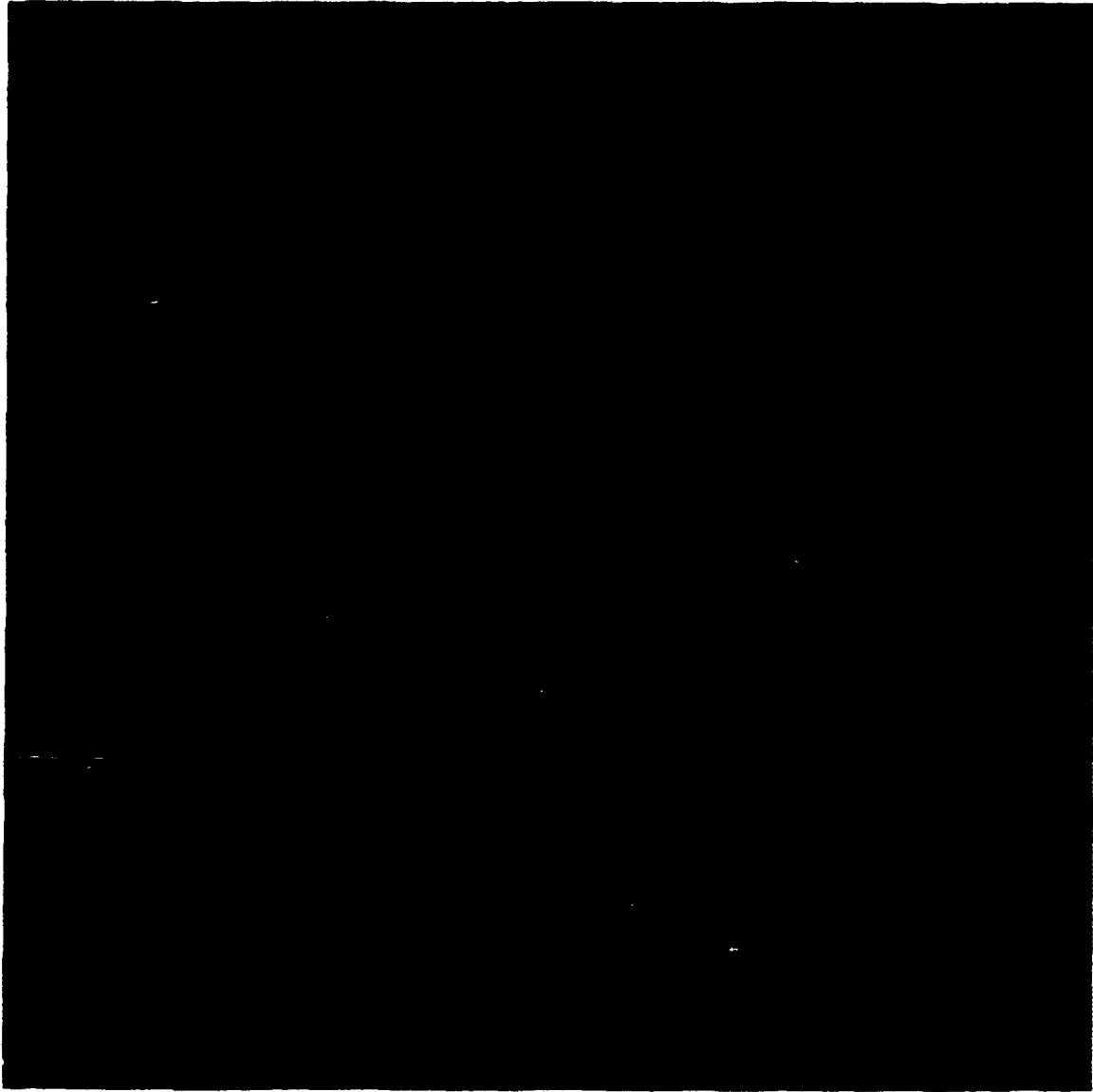


Figure 34. Two-dimensional gray scale pictorial representation of 1024 x 1024 ARMA simulated data with low frequencies subtracted (as in Figure 33). The data set was constructed for  $L_c = 84$  km, 2-D slope =  $-8/3$ , spacing = 100 m, AR order =  $3 \times 3$ , and MA order =  $7 \times 7$

```

LC= 8.48E-01 SIGMA=6.00E-08 SLOPE OF PSD=-2.67
A= 1.48E-08 HEIGHT LOWEST PRED BY 1.00E-02 USED FOR R.N.=31111
AR ORDER 3 X 3   RA ORDER 7 X 7
ITERATE FOR AR 40 20 TIMES RANGE OF VALUES IN SCENE -1.07E-01 THRU 1.24E-01
MIN. F.../(IN...)= 7.81E-02 WHERE N=128   AND OR= 1.00E-01
SIMULATE SCENE 1024 BY 1024 FROM ORIGINAL 1300 BY 1300
REPLACE      12  12 FREQUENCIES.   SPECIFIC FREQUENCY 1/(10*1024)
IGNORE FREQUENCY 0.0

```

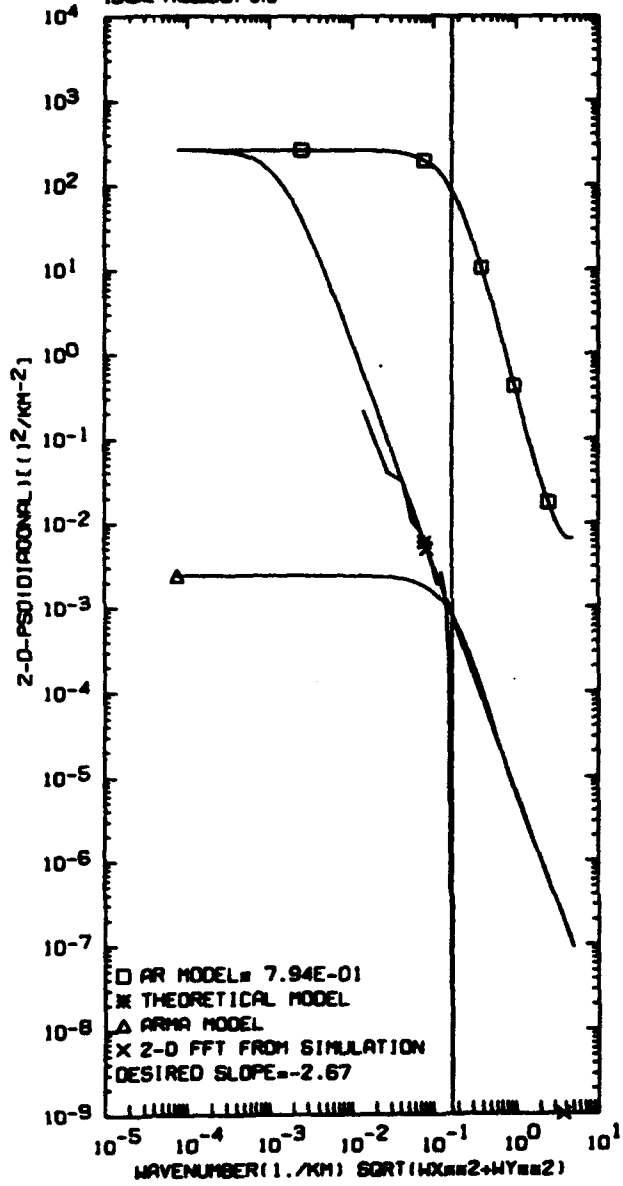
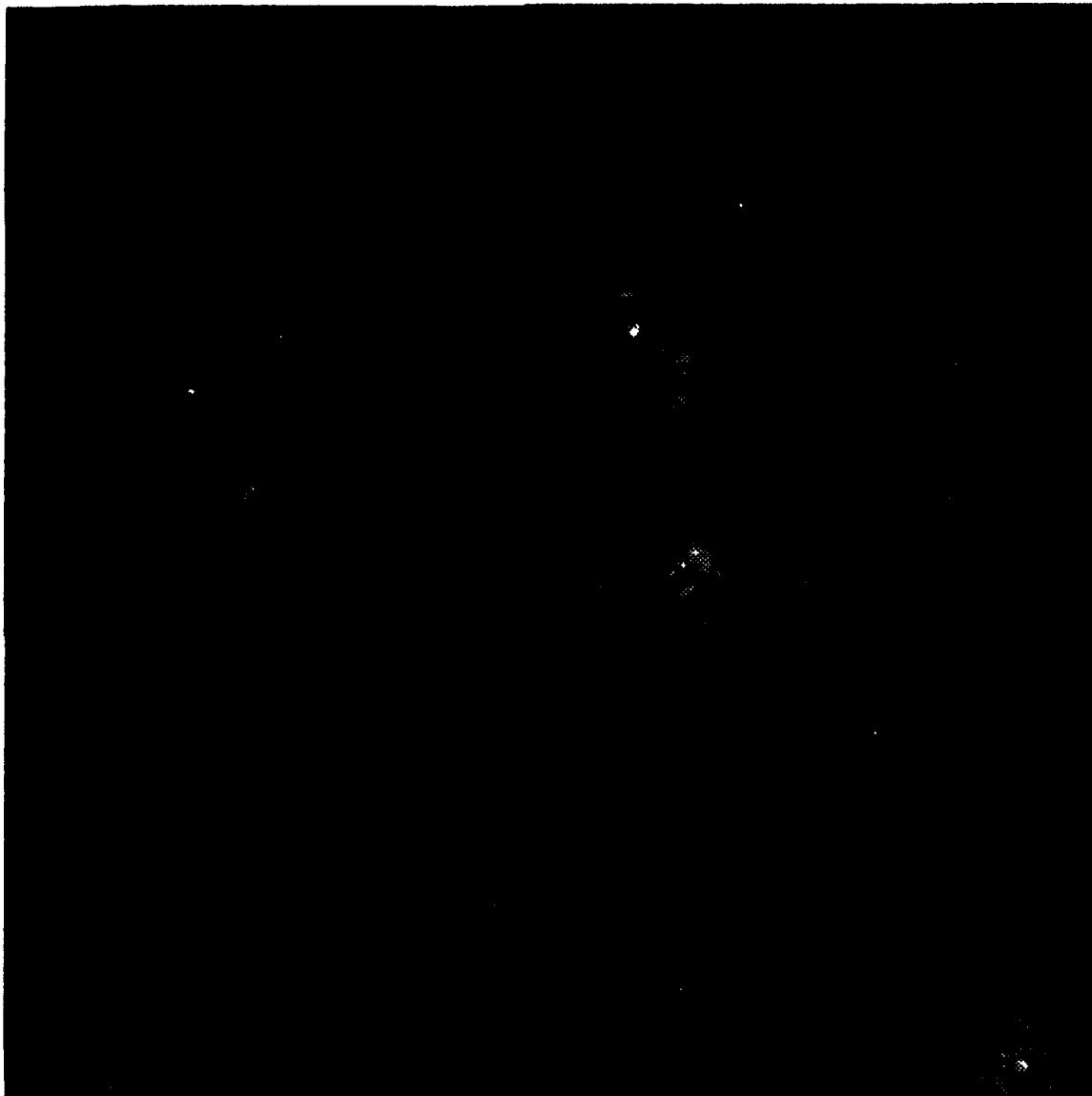


Figure 35. Same as Figure 29, except only the DFT low frequency replacement power values are shown in the simulation



**Figure 36.** Two-dimensional gray scale pictorial representation of 1024 x 1024 ARMA simulated data (corresponds to Figure 29). The data set was constructed for  $L_c = 84$  km, 2-D slope =  $-8/3$ , spacing = 100 m, AR order = 3 x 3, and MA order = 7 x 7

## 7. CONVENTIONAL SIMULATION - RESULTS AND DISCUSSION

This section focuses on comparing the 2-D ARMA results with a corresponding simulation obtained by invoking the conventional fast Fourier transform method. The FFT method is straightforward in that: (a) we calculate the FFT of  $\epsilon(x,y)$ , where  $\epsilon(x,y)$  is chosen to be the same set of Gaussian random numbers that we used in calculating the ARMA simulation; (b) multiply by the desired filter (that is, the square root of the desired PSD,  $F(f_x, f_y)$ , divided by the spacing,  $T_1$ ); and (c), perform the inverse FFT. Where  $g(x,y)$  comprises the conventional 2-D simulation, the process is described by:

$$g(x,y) = \text{ifft} \left[ \left\{ \text{fft}(\epsilon(x,y)) \right\} \times \frac{\sqrt{F(f_x, f_y)}}{T_1} \right].$$

Figure 37 shows a two dimensional periodogram of data simulated by using this technique. The log-log plot shows the two-dimensional power spectral density (PSD) versus spatial frequency plotted along a diagonal. The curve marked by an asterisk (\*) is the desired or "theoretical" PSD and the curve marked by an X is the 2-D PSD obtained from the 1024 x 1024 FFT simulated data set. The "theoretical" 2-D slope is -2.67 and the correlation length  $L_c = 84$  km. Figure 37 thus corresponds to the ARMA plot in Figure 29. Examination of these plots show that the ARMA and FFT simulation methods appear to yield very similar PSD's.

Figure 38 shows a one-dimensional periodogram of the two-dimensional data set just described. The log-log plot shows the 1-D power spectral density (PSD) versus spatial frequency plotted along a major axis. Again, the curve marked by an asterisk (\*) is the desired or "theoretical" 1-D PSD and the curve marked by X's represents the 1D periodogram derived from the rows and columns of the 2-D simulated data corresponding to Figure 37. Not unexpectedly, good agreement obtains between the "theoretical" 1-D PSD and the PSD of the FFT generated data set.

For completeness, Figure 39 shows a two-dimensional gray scale pictorial realization of 102.4 x 102.4 km FFT simulated data corresponding to Figure 37. The structured data was constructed for  $L_c = 84$  km, 2-D slope = -8/3, and spacing = 100 m. Comparison of the 2-D ARMA gray scale plot (Figure 36) with Figure 39 provides visual (though subjective) evidence of the ability of the ARMA method and FFT method to generate equivalent structured scenes.

LC= 0.48E+01 SIGMA=0.00E+00 SLOPE OF PSD=-2.67  
 No 1.48E+00 SEED FOR R.N.=31111  
 USE FFT TO SIMULATE RANGE OF VALUES IN SCENE 0.00E+00 THRU 0.00E+00  
 SIMULATE SCENE 1024 BY 1024 SIZE 1.00E+01

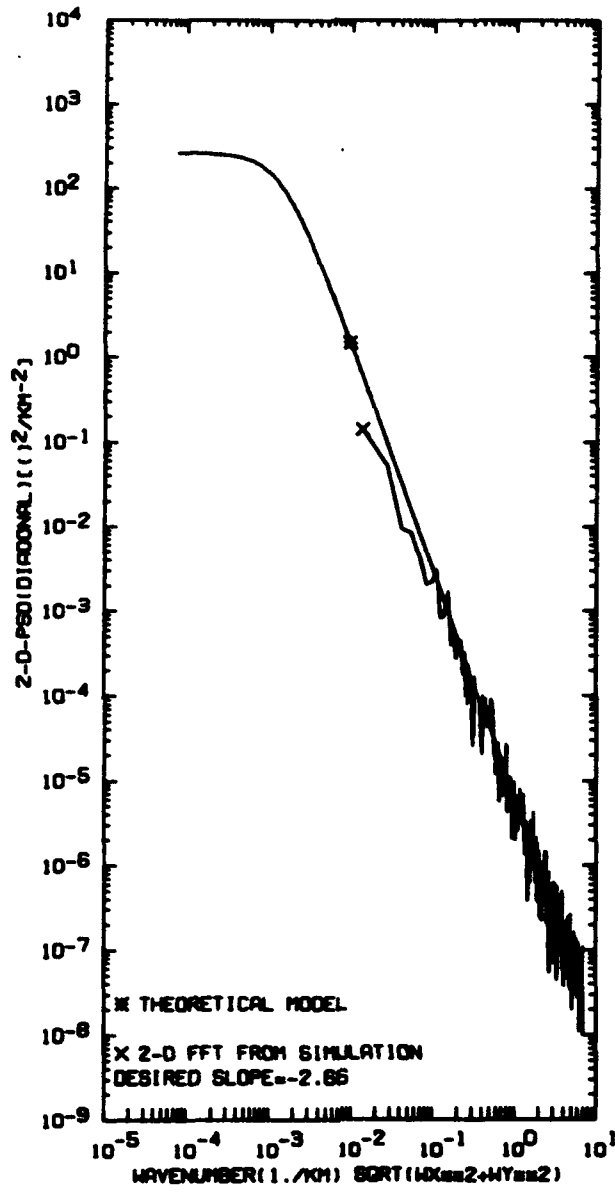


Figure 37. Log-log plot of two-dimensional power spectral density (PSD) versus spatial frequency plotted along a diagonal. Curve marked by an asterisk (\*) is the desired or "theoretical" PSD. Curve marked by an X is a 2-D PSD of a 2-D sheet of data derived from conventional (that is, FFT) simulation. The 1024 x 1024 simulated data set was derived by performing FFT operations on the same set of random numbers as obtained for Figure 29. The "theoretical" 2-D slope is -2.67 and the correlation length  $L_c = 84$  km

$L_C = 0.40E+01$   $SIGMA_{1-D} = 0.00E+00$  SLOPE OF PSD = 1.67  
 No. 1.00E+00 USED FOR R.N. = 01111  
 USE FFT TO SIMULATE RANGE OF VALUES IN SCENE 0.00E+00 TO 0.00E+00  
 SIMULATE SCENE 1004 BY 1004 SIZE 1.00E+01

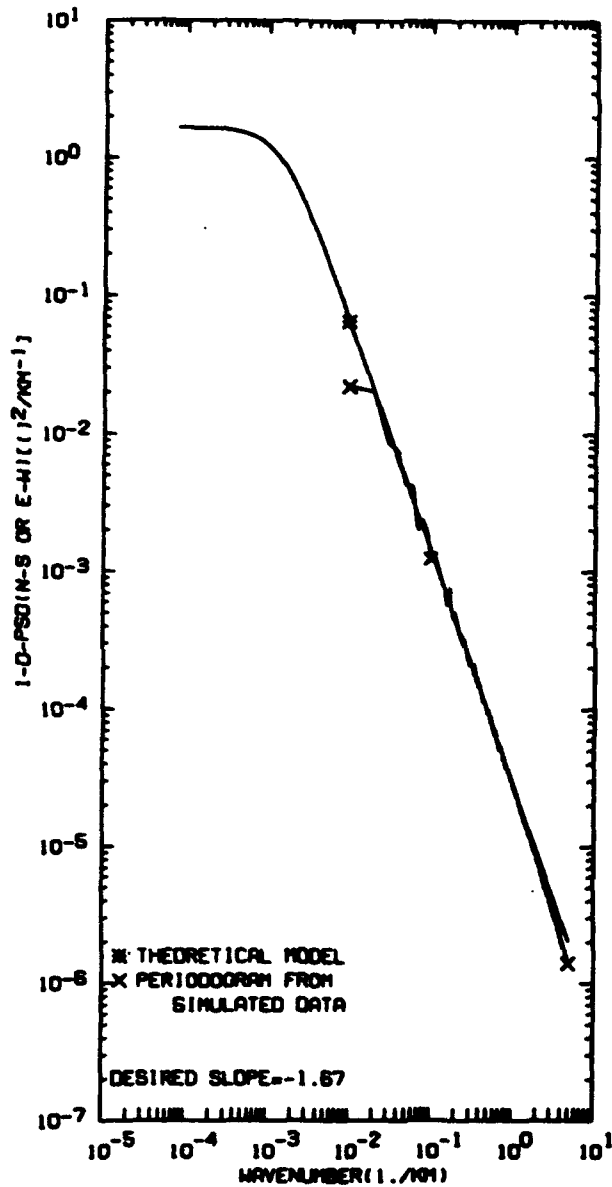
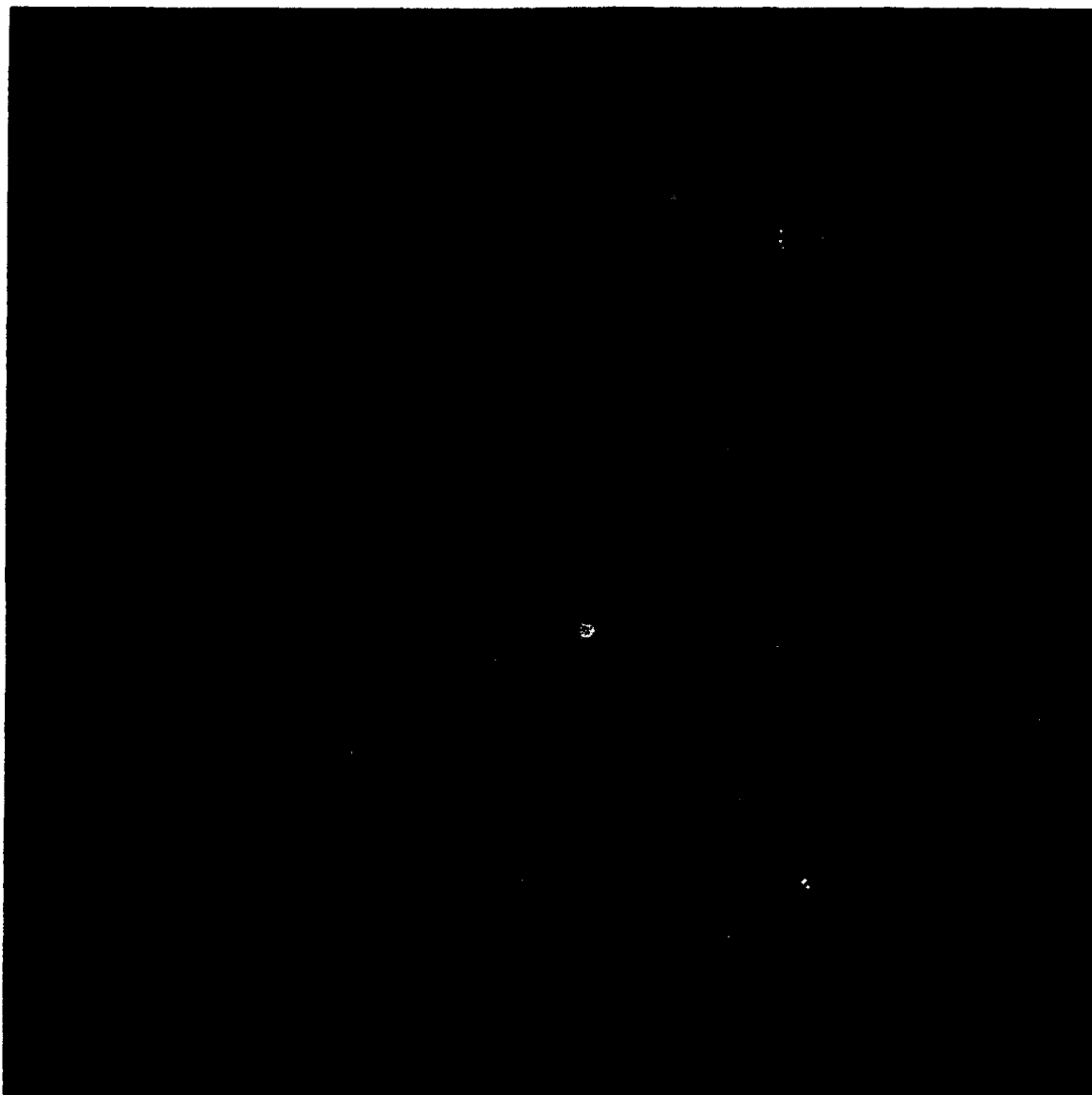


Figure 38. Log-log plot of one-dimensional power spectral density (PSD) versus spatial frequency plotted along a major axis. Curve marked by an asterisk (\*) is the desired or "theoretical" 1-D PSD. Curve marked by X's represents the 1D periodogram derived from the rows and columns of the 2-D FFT simulated data corresponding to Figure 37. The "theoretical" 1-D slope is -1.67 and the correlation length  $L_C = 84$  km



**Figure 39. Two-dimensional gray scale pictorial representation of 1024 x 1024 FFT simulated data (corresponds to Figure 37). The data set was constructed for  $L_c = 84$  km, 2-D slope =  $-8/3$ , spacing = 100 m**

## 8. COMPUTATIONAL BURDEN

As mentioned in the introduction, enormous computer time is consumed in constructing realistic but practical three dimensional maps of atmospheric temperature or density fluctuations from conventional analysis techniques. It is necessary therefore to explore alternative means of constructing structure maps while reducing the computational burden. Although the present work succeeded in providing a reliable alternative method, it did not realize the goal of reducing the computational burden. This work does, however, point to the possibility of using a hybrid FFT/AR three-dimensional technique that promises significant computer savings. This idea will be explored in a subsequent report.

The computer timings for calculations in this report were measured on the Phillips Laboratory model 210 Convex computer. In solving for the ARMA filter coefficients, it was found that most of the time was spent calculating the MA terms. For example, solving for a 3 x 3 AR filter took 1.2 s and solving for a 13 x 13 AR filter took 3.0 s but solving for a 25 x 25 MA filter took 12.3 s. Table 1 however shows that these times are small compared to the time needed to construct a simulation given the filter coefficients. For example, it took  $10^4$  seconds to simulate 1300 x 1300 data points using an order 13 x 13 AR and order 25 x 25 MA filter. In contrast to the time required to construct the ARMA simulations, Table 1 shows that less than 56 seconds were required to perform a conventional 2-D FFT simulation corresponding to Figure 37 (due to our self-imposed constraint of using sections of the aforementioned ARMA program, approximately 28 percent of the time is excess overhead). Even the low order 3 x 3 AR and 7 x 7 MA filter took nearly ten times as long to process as the conventional method. Thus the FFT technique proves much faster than the 2-D ARMA modern spectral analysis method in constructing comparable 2-D structure.

Table 1. Timing of Simulations

	1300 x 1300 ARMA (seconds)	1024 x 1024 FFT (seconds)
13 x 13 AR (10 cycles) & 25 x 25 MA	approx. $1 \times 10^4$ s	< 56 s
3 x 3 AR (10 cycles) & 31 x 31 MA	approx. $1 \times 10^3$ s	< 56 s
21 x 21 AR (10 cycles) & 31 x 31 MA	approx. $3 \times 10^4$ s	< 56 s
3 x 3 AR (20 cycles) & 7 x 7 MA with DFT replacement	approx. 580 s	< 56 s

## 9. CONCLUSIONS

Because geophysical data often are characterized by smooth continuous power spectral density functions, this report has explored the possibility of generating two-dimensional synthetic structure scenes by passing stochastic data through an autoregressive/moving average filter having the characteristics of the desired two-dimensional PSD.

Several alternative procedures were developed to construct ARMA filters that covered a broad frequency range, and featured near circular symmetry. A combination of quarter plane and full plane autoregressive filters cascaded with a moving average filter coupled with low frequency discrete Fourier transform power replacement proved satisfactory and effective in generating high fidelity power spectral density functions. Simulated in this way, the two-dimensional power spectral density functions of several scene realizations closely matched the desired or "theoretical" PSD. As observed, PSD's having a small slope, large correlation length, and small data spacing were more difficult to model than PSD's with larger slope, smaller correlation length, and wider data spacing. The analysis indicated that two-dimensional isotropic horizontal atmospheric temperature structure, having a data spacing of 100 m and a characteristically smooth power spectral density can be modeled within a frequency band ranging from  $0.08 \text{ km}^{-1}$  to  $5 \text{ km}^{-1}$  by an autoregressive  $3 \times 3$  order process and a moving average  $7 \times 7$  order process. DFT replacement allowed extension of the lower frequency bound to  $0.01 \text{ km}^{-1}$ . At the expense of increasing computer time, one may increase the frequency range without DFT replacement and achieve agreement to  $0.01 \text{ km}^{-1}$  by choosing a  $13 \times 13$  AR model and  $25 \times 25$  MA model. Synthetic scenes generated by the ARMA process maintained high fidelity to the "theoretical" PSD's for two-dimensional spectral slopes ranging from  $-8/3$  to  $-11/3$  and correlation lengths ranging from 32 to 84 km. Comparison with a conventional technique (Fast Fourier Transform), showed that the ARMA and FFT simulation methods appear to yield similar power spectral density functions and visual two-dimensional scenes.

A reliable alternative procedure was developed to produce structure arrays having circularly symmetric power spectral densities that matched desired geophysical specifications. The procedure accounts for the isotropic horizontal correlation scales, including the line-of-sight, that existing models approximate. The computational burden of the ARMA iterative process proved more severe than the conventional FFT technique for large correlation scales. The process that was eventually chosen led to run times 10 times the execution time of the 2-D FFT process. Despite the success of the model in achieving fidelity to filter specifications, it is hoped this report will serve as a detailed study in 2-D ARMA analysis for a particular geophysical condition, and as a caution to the ability of method to achieve computer savings. This and the previous work does, however, point to the favorability of using a hybrid FFT/AR three-dimensional technique that promises to have economical computer savings. This idea will be explored in a subsequent report.



## References

1. Sharma, R.D., Duff, J.W., Sundberg, R.L., Gruninger, J.H., Bernstein, L.S., Robertson, D.C., and Healey, R.J., (1991) *Description of SHARC-2, The Strategic High Altitude Atmospheric Radiance Code*, Phillips Laboratory technical report, PL-TR-91-2071.ADA239008
2. Brown, J.H., (1993) *Atmospheric Structure Simulation: An Autoregressive Model for Smooth Geophysical Power Spectra with Known Autocorrelation Function*, Phillips Laboratory technical report, PL-TR-93-2185, ERP #1128. ADA276691
3. Marple, S.L. (1987) *Digital Spectral Analysis with Applications*, Chapter 6, Prentice-Hall, Englewood Cliffs, New Jersey.
4. Kay, Steven M.,(1988) *Modern Spectral Estimation, Theory & Application*, Prentice-Hall, Englewood Cliffs, New Jersey.
5. Lim, J.S. (1990) *Two-Dimensional Signal and Image Processing*, Prentice-Hall, Englewood Cliffs New Jersey, , pg 269.
6. Strugala, L.A., Newt, J.E., Futterman, W., Schweitzer, E.L., Herman, B.J., and Sears, R.D.(1991) *Development of High Resolution Statistically Non-stationary Infrared Earthlimb Radiance Scenes, Characterization, Propagation, and Simulation of Sources and Backgrounds, Proceedings SPIE - The International Society for Optical Engineering, V1486, pp 176-187, April 1991, Orlando, Florida.*



## Appendix

### Computational Details

#### ANALYSIS OF SUMMING FOUR SYMMETRICAL QUARTER PLANE FILTERS

$$\begin{aligned} \frac{1}{A_{A1}(f_x, f_y)} &= \frac{1}{\sum_{m=-M}^M \sum_{n=-N}^N a_1(m, n) (\cos(2\pi T_1(mf_x + nf_y)) - i \sin(2\pi T_1(mf_x + nf_y)))} \\ &= \frac{\sum_{m=-M}^M \sum_{n=-N}^N a_1(m, n) (\cos(2\pi T_1(mf_x + nf_y)) + i \sin(2\pi T_1(mf_x + nf_y)))}{\left( \sum_{m=-M}^M \sum_{n=-N}^N a_1(m, n) \{\cos[2\pi T_1(mf_x + nf_y)]\} \right)^2 + \left( \sum_{m=-M}^M \sum_{n=-N}^N a_1(m, n) \{\sin[2\pi T_1(mf_x + nf_y)]\} \right)^2} \end{aligned}$$

Looking at the numerators,  $N_1$  and  $N_4$  of  $\frac{1}{A_{A1}}$  and  $\frac{1}{A_{A4}}$ , we observe,

$$N_1 = \sum_{m=0}^M \sum_{n=0}^N a_1(m, n) \{\cos[2\pi T_1(mf_x + nf_y)] + i \sin[2\pi T_1(mf_x + nf_y)]\}$$

$$N_4 = \sum_{m=-M}^0 \sum_{n=-N}^0 a_4(m, n) \{\cos[2\pi T_1(mf_x + nf_y)] + i \sin[2\pi T_1(mf_x + nf_y)]\}$$

but  $a_1(m, n) = a_4(-m, -n)$

so,

$$N_4 = \sum_{m=0}^M \sum_{n=0}^N a_4(m, n) \{\cos[2\pi T_1(-mf_x - nf_y)] + i \sin[2\pi T_1(-mf_x - nf_y)]\}$$

so that,

$$N_1 + N_4 = 2 \sum_{m=0}^M \sum_{n=0}^N a_1(m, n) \cos[2\pi T_1(mf_x + nf_y)]$$

Looking at the denominators  $D_1$  and  $D_4$  of  $\frac{1}{A_{A1}}$  and  $\frac{1}{A_{A4}}$ , we observe,

$$D_1 = \left\{ \sum_{m=0}^M \sum_{n=0}^N a_1(m,n) \cos[2\pi T_1(mf_x + nf_y)] \right\}^2 + \left\{ \sum_{m=0}^M \sum_{n=0}^N a_1(m,n) \sin[2\pi T_1(mf_x + nf_y)] \right\}^2$$

$$D_4 = \left\{ \sum_{m=-M}^0 \sum_{n=-N}^0 a_4(m,n) \cos[2\pi T_1(mf_x + nf_y)] \right\}^2 + \left\{ \sum_{m=-M}^0 \sum_{n=-N}^0 a_4(m,n) \sin[2\pi T_1(mf_x + nf_y)] \right\}^2$$

but,  $a_1(m,n) = a_4(-m,-n)$ , so that,

$$D_4 = \left( \sum_{m=0}^M \sum_{n=0}^N a_1(m,n) \cos(2\pi T_1(-mf_x - nf_y)) \right)^2 + \left( \sum_{m=0}^M \sum_{n=0}^N a_1(m,n) \sin(2\pi T_1(-mf_x - nf_y)) \right)^2$$

so that,  $D_1 = D_4$

consequently,

$$\frac{1}{A_{A1}} + \frac{1}{A_{A4}} = \frac{2 \sum_{m=0}^M \sum_{n=0}^N a_1(m,n) \cos[2\pi T_1(mf_x + nf_y)]}{\left\{ \sum_{m=0}^M \sum_{n=0}^N a_1(m,n) \cos[2\pi T_1(mf_x + nf_y)] \right\}^2 + \left\{ \sum_{m=0}^M \sum_{n=0}^N a_1(m,n) \sin[2\pi T_1(mf_x + nf_y)] \right\}^2}$$

Likewise looking at the numerators,  $N_2$  and  $N_3$  of  $\frac{1}{A_{A2}}$  and  $\frac{1}{A_{A3}}$ , we observe,

$$N_2 = \sum_{m=-M}^0 \sum_{n=0}^N a_2(m,n) \left\{ \cos[2\pi T_1(mf_x + nf_y)] + i \sin[2\pi T_1(mf_x + nf_y)] \right\}$$

but  $a_2(-m,n) = a_3(m,-n)$

So,

$$N_2 = \sum_{m=0}^M \sum_{n=0}^N a_2(-m,n) \left\{ \cos[2\pi T_1(-mf_x + nf_y)] + i \sin[2\pi T_1(-mf_x + nf_y)] \right\}$$

$$N_3 = \sum_{m=0}^M \sum_{n=0}^N a_3(m,-n) \left\{ \cos[2\pi T_1(mf_x - nf_y)] + i \sin[2\pi T_1(mf_x - nf_y)] \right\}$$

but  $a_3(m,-n) = a_2(-m,n) = a_1(m,n)$

so that,

$$N_2 + N_3 = 2 \sum_{m=0}^M \sum_{n=0}^N a_1(m,n) \cos[2\pi T_1(mf_x - nf_y)]$$

Looking at the denominators  $D_2$  and  $D_3$  of  $\frac{1}{A_{A2}}$  and  $\frac{1}{A_{A3}}$ , we observe.

$$D_2 = \left\{ \sum_{m=-M}^0 \sum_{n=0}^N a_2(m, n) \cos[2\pi T_1(mf_x + nf_y)] \right\}^2 + \left\{ \sum_{m=-M}^0 \sum_{n=0}^N a_2(m, n) \sin[2\pi T_1(mf_x + nf_y)] \right\}^2$$

$$D_2 = \left\{ \sum_{m=0}^M \sum_{n=0}^N a_2(-m, n) \cos[2\pi T_1(-mf_x + nf_y)] \right\}^2 + \left\{ \sum_{m=0}^M \sum_{n=0}^N a_2(-m, n) \sin[2\pi T_1(-mf_x + nf_y)] \right\}^2$$

$$D_3 = \left\{ \sum_{m=0}^M \sum_{n=-N}^0 a_3(m, n) \cos[2\pi T_1(mf_x + nf_y)] \right\}^2 + \left\{ \sum_{m=0}^M \sum_{n=-N}^0 a_3(m, n) \sin[2\pi T_1(mf_x + nf_y)] \right\}^2$$

$$D_3 = \left\{ \sum_{m=0}^M \sum_{n=0}^N a_3(m, -n) \cos[2\pi T_1(mf_x - nf_y)] \right\}^2 + \left\{ \sum_{m=0}^M \sum_{n=0}^N a_3(m, -n) \sin[2\pi T_1(mf_x - nf_y)] \right\}^2$$

but  $a_2(-m, n) = a_3(m, -n) = a_1(m, n)$

so that,  $D_2 = D_3$

consequently,

$$\frac{1}{A_{A2}} + \frac{1}{A_{A3}} = \frac{2 \sum_{m=0}^M \sum_{n=0}^N a_1(m, n) \cos[2\pi T_1(mf_x - nf_y)]}{\left\{ \sum_{m=0}^M \sum_{n=0}^N a_1(m, n) \cos[2\pi T_1(mf_x - nf_y)] \right\}^2 + \left\{ \sum_{m=0}^M \sum_{n=0}^N a_1(m, n) \sin[2\pi T_1(mf_x - nf_y)] \right\}^2}$$

Finally

$$\frac{1}{A_A} = \frac{2 \sum_{m=0}^M \sum_{n=0}^N a_1 \cos[2\pi T_1(mf_x + nf_y)] \quad 2 \sum_{m=0}^M \sum_{n=0}^N a_1 \cos[2\pi T_1(mf_x - nf_y)]}{\left\{ \sum_{m=0}^M \sum_{n=0}^N \cos[2\pi T_1(mf_x + nf_y)] \right\}^2 + \left\{ \sum_{m=0}^M \sum_{n=0}^N \sin[2\pi T_1(mf_x + nf_y)] \right\}^2 + \left\{ \sum_{m=0}^M \sum_{n=0}^N \cos[2\pi T_1(mf_x - nf_y)] \right\}^2 + \left\{ \sum_{m=0}^M \sum_{n=0}^N \sin[2\pi T_1(mf_x - nf_y)] \right\}^2}$$

Ignoring the sine terms for  $f_x \rightarrow 0$ , and  $f_y \rightarrow 0$ :

$$\frac{1}{A_A} \sim \frac{\sum_{m=0}^M \sum_{n=0}^N a_1(m,n) \cos[2\pi T_1(mf_x + nf_y)]}{\sum_{m=0}^M \sum_{n=0}^N a_1(m,n) [\cos(2\pi mf_x T_1) \cos(2\pi nf_y T_1) - \sin(2\pi mf_x T_1) \sin(2\pi nf_y T_1)]} = \frac{\sum_{m=0}^M \sum_{n=0}^N a_1(m,n) [\cos(2\pi mf_x T_1) \cos(2\pi nf_y T_1)]}{\sum_{m=0}^M \sum_{n=0}^N a_1(m,n) [\cos(2\pi mf_x T_1) \cos(2\pi nf_y T_1)]}$$

where, again we have ignored sine terms. This implies that as  $f_x \rightarrow 0$ , and  $f_y \rightarrow 0$ , and checking the definition of  $a_1(m,n)$ , we see as before, the following approximation:  $\frac{1}{A_A(f_x, f_y)} \sim \frac{4}{A(f_x, f_y)}$ . It is unclear why the sum of the quarter plane filters performs better than the average.

#### ANALYSIS OF LOW FREQUENCY DFT REPLACEMENT

The following describes the analysis and procedure for subtracting the low frequency components of the 2-D ARMA simulated scene.

Assume that  $G(x,y)$  is a two-dimensional sheet of simulated data. We wish to find the discrete Fourier coefficients  $A(\omega_1, \omega_2)$  at frequencies  $\omega_1$  and  $\omega_2$  where,

$$\omega_1 = 0, \pm \frac{2\pi}{N}, \pm 2\left(\frac{2\pi}{N}\right), \pm 3\left(\frac{2\pi}{N}\right), \dots, \pm \pi$$

$$\omega_2 = 0, \pm \frac{2\pi}{N}, \pm 2\left(\frac{2\pi}{N}\right), \pm 3\left(\frac{2\pi}{N}\right), \dots, \pm \pi$$

but not  $\omega_1 = \omega_2 = 0$  or  $|\omega_1| = |\omega_2| = \pi$ . Then,

$$A(\omega_1, \omega_2) = \frac{2}{N^2} \sum_x \sum_y G(x,y) e^{-i\omega_1 x} e^{-i\omega_2 y}$$

and,

$$A(-\omega_1, -\omega_2) = \frac{2}{N^2} \sum_x \sum_y G(x,y) e^{i\omega_1 x} e^{i\omega_2 y}$$

$$= A^*(\omega_1, \omega_2)$$

So, where  $\Re$  signifies the real components, and  $\Im$  signifies the imaginary components:

$$\begin{aligned}\Re A(\omega_1, \omega_2) &= \Re A(-\omega_1, -\omega_2) \\ &= \frac{2}{N^2} \sum_x \sum_y G(x, y) [\cos(\omega_1 x) \cos(\omega_2 y) - \sin(\omega_1 x) \sin(\omega_2 y)]\end{aligned}$$

and,

$$\begin{aligned}\Im A(\omega_1, \omega_2) &= -\Im A(-\omega_1, -\omega_2) \\ &= \frac{2}{N^2} \sum_x \sum_y G(x, y) [\cos(\omega_1 x) \sin(\omega_2 y) + \sin(\omega_1 x) \cos(\omega_2 y)]\end{aligned}$$

Now the contribution of  $A(\omega_1, \omega_2)$  at point  $x, y$  is:

$$\begin{aligned}C(x, y) &= \Re[A(\omega_1, \omega_2)] [\cos(\omega_1 x) \cos(\omega_2 y) - \sin(\omega_1 x) \sin(\omega_2 y)] \\ &\quad + \Im[A(\omega_1, \omega_2)] [\cos(\omega_1 x) \sin(\omega_2 y) + \sin(\omega_1 x) \cos(\omega_2 y)]\end{aligned}$$

and the contribution of  $A(-\omega_1, -\omega_1)$  at point  $x, y$  is:

$$\begin{aligned}&= \Re[A(-\omega_1, -\omega_2)] [\cos(\omega_1 x) \cos(\omega_2 y) - \sin(\omega_1 x) \sin(\omega_2 y)] \\ &\quad + \Im[A(-\omega_1, -\omega_2)] [-\cos(\omega_1 x) \sin(\omega_2 y) - \sin(\omega_1 x) \cos(\omega_2 y)]\end{aligned}$$

and since  $A(\omega_1, \omega_2) = A^*(-\omega_1, -\omega_2)$ , the contribution of  $A(\omega_1, \omega_2) + A(-\omega_1, -\omega_2)$  is :

$$\begin{aligned}CC(x, y) &= 2\Re[A(\omega_1, \omega_2)] [\cos(\omega_1 x) \cos(\omega_2 y) - \sin(\omega_1 x) \sin(\omega_2 y)] \\ &\quad + 2\Im[A(\omega_1, \omega_2)] [\cos(\omega_1 x) \sin(\omega_2 y) + \sin(\omega_1 x) \cos(\omega_2 y)]\end{aligned}$$

Taking the subset of frequencies:

$$-11\left(\frac{2\pi}{N}\right) \leq \omega_1 \leq 11\left(\frac{2\pi}{N}\right) \quad \text{and} \quad 0 \leq \omega_2 \leq 11\left(\frac{2\pi}{N}\right) \quad \text{but not } \omega_1 = \omega_2 = 0$$

(we call this a 12 x 12 or L x L subset of frequencies) we subtract CC(x,y) at these frequencies from G(x,y) and add instead the DD(x,y) values described below.

The following describes the analysis and procedure for replacing the low frequency components to the simulated scene.

We set up an array of  $2L \times 2L$  pseudo-random numbers  $\epsilon(s,t)$  drawn from a Gaussian probability distribution with standard deviation = 1 and then calculate the 2-D FFT of  $\epsilon(s,t)$ ,  $G(\omega_3, \omega_4)$ , where,

$$\begin{cases} \omega_3 = \frac{2\pi T}{2L} \\ \omega_4 = \frac{2\pi T}{2L} \end{cases} \left\{ -L \leq T \leq L. \right.$$

Invoking Pascal's theorem, the expected value of the square of the amplitudes of  $G(\omega_3, \omega_4)$  is  $(2L)^2$ . But  $G(\omega_3, \omega_4)$  has the proper functional form of the probability density function for the Fourier transform of the data we wish to simulate. The idea is to take a value of  $G(\omega_3, \omega_4)$  and multiply it by a value  $M(\omega_1, \omega_2)$  to get the expected value of  $A(\omega_1, \omega_2)$  which will have the power spectral density we wish to simulate. This means:

$$\overline{|GG(\omega_3, \omega_4)|^2} [M(\omega_1, \omega_2)]^2 = \frac{F(\omega_1, \omega_2)}{(\Delta x)^2 (N^2)}$$

where  $F(\omega_1, \omega_2)$  is the power spectral density we are trying to

simulate and  $\Delta x = 100$  m is the spacing of the data we are simulating. Thus,

$$(2L)^2 [M(\omega_1, \omega_2)]^2 = \frac{F(\omega_1, \omega_2)}{(\Delta x)^2 (N^2)}$$

or,

$$M(\omega_1, \omega_2) = \frac{\sqrt{F(\omega_1, \omega_2)}}{2 \times \Delta x \times L \times N}$$

and,

$$D(\omega_1, \omega_2) = GG\left(\frac{N\omega_1}{2L}, \frac{N\omega_2}{2L}\right) * M(\omega_1, \omega_2)$$

Then, as above, the contribution at point  $(x,y)$  of  $D(\omega_1, \omega_2) + D(-\omega_1, -\omega_2)$  is :

$$\begin{aligned} DD(x, y) = & 2\Re[D(\omega_1, \omega_2)] [\cos(\omega_1 x) \cos(\omega_2 y) - \sin(\omega_1 x) \sin(\omega_2 y)] \\ & + 2\Im[D(\omega_1, \omega_2)] [\cos(\omega_1 x) \sin(\omega_2 y) + \sin(\omega_1 x) \cos(\omega_2 y)] \end{aligned}$$